Using half-metallic manganite interfaces to reveal insights into spintronics

2007 J. Phys.: Condens. Matter 19 315208

(http://iopscience.iop.org/0953-8984/19/31/315208)

IOP PUBLISHING JOURNAL OF PHYSICS: CONDENSED MATTER

J. Phys.: Condens. Matter **19** (2007) 315208 (27pp) doi:10.1088/0953-8984/19/31/315208

Using half-metallic manganite interfaces to reveal insights into spintronics

M Bowen[1,2], J-L Maurice[2], A Barthélémy[2], M Bibes[7], D Imhoff[4], V Bellini[4,5], R Bertacco[6], D Wortmann[4], P Seneor[2], E Jacquet[2], A Vaurès[2], J Humbert[2], J-P Contour[2], C Colliex[3], S Blügel[4] and P H Dederichs[4]

[1] Institut de Physique et Chimie des Matériaux de Strasbourg (IPCMS), UMR 7504 CNRS-ULP, 23 rue du Loess BP 43, 67034 Strasbourg, France
[2] Unité Mixte de Physique CNRS/Thales, Route Départementale 128, 91767 Palaiseau Cedex, France
and
Université de Paris-Sud XI, 91405 Orsay Cedex, France
[3] Laboratoire de Physique des Solides, Bâtiment 510, Université de Paris-Sud XI, 91405 Orsay, France
[4] Institut für Festkörperforschung, Forschungszentrum Jülich, D-52425 Jülich, Germany
[5] CNISM and CNR-INFM-S3, Department of Physics, University of Modena and Reggio Emilia, Via Campi 213/A, 41100 Modena, Italy
[6] Dipartimento di Fisica del Politecnico di Milano, INFM and L-NESS, via Anzani 52, 22100 Como, Italy

E-mail: Martin.Bowen@ipcms.u-strasbg.fr

Received 20 November 2006, in final form 25 January 2007
Published 3 July 2007
Online at stacks.iop.org/JPhysCM/19/315208

Abstract

A half-metal has been defined as a material with propagating electron states at the Fermi energy only for one of the two possible spin projections, and as such has been promoted as an interesting research direction for spin electronics. This review details recent advances on manganite thin film research within the field of spintronics, before presenting the structural, electronic and spin-polarized solid-state tunnelling transport studies that we have performed on heterostructures involving $La_{2/3}Sr_{1/3}MnO_3$ thin films separated by $SrTiO_3$ barriers. These experiments demonstrate that, with a polarization of spin $\uparrow$ electrons at the Fermi level that can reach 99%, the $La_{2/3}Sr_{1/3}MnO_3/SrTiO_3$ interface for all practical purposes exhibits half-metallic behaviour. We offer insight into the electronic structure of the interface, including the electronic symmetry of any remaining spin $\downarrow$ states at the Fermi level. Finally, we present experiments that use the experimental half-metallic property of manganites as tools to reveal novel features of spintronics.

(Some figures in this article are in colour only in the electronic version)

[7] Present address: Institut d'Electronique Fondamentale, Bâtiment 220, Université de Paris-Sud XI, 91405 Orsay, France.

Contents

1. Introduction

The beginnings of the field of spin electronics, or spintronics, were undertaken with the complementary discovery in 1986 of magnetic interlayer exchange coupling (IEC) by the Grünberg group [1] and in 1988 of giant magnetoresistance (GMR) by the Fert group [2] on heterostructures that consist of alternating ferromagnetic and metallic thin films. Both effects are in part the result of an imbalance at the Fermi level E_F between the electron populations N with the two possible quantum mechanical spin projections $\uparrow$ and $\downarrow$, an imbalance that is naturally present in ferromagnetic materials—$N_\uparrow \neq N_\downarrow$. The spin polarization P of the conduction electrons, i.e. at E_F, in such ferromagnets (FMs) can then be defined in terms of these densities of states (DOSs) as:

$$P(E_F) = \frac{N^\uparrow(E_F) - N^\downarrow(E_F)}{N^\uparrow(E_F) + N^\downarrow(E_F)}. \quad (1)$$

Since these paramount discoveries, the field of spintronics [3] has progressed considerably, so as to understand the importance of the electronic properties of the metallic spacer layer that is used [4]. An initially distinct branch of spintronics that integrates a semiconducting or insulating (I) spacer was reasserted through pioneering experiments in 1995 on magnetic tunnel junctions (MTJs) [5]. In fact, a convergence between these two branches of spintronics has recently begun to emerge [6–10] and should propel the coalesced field into new research directions. In this vein, a nascent yet rising research effort is currently underway to leverage the physical concepts of spintronics across metallic and insulating spacers, alongside the field of organic/molecular electronics [11–13], toward developing the spintronics of organic semiconductor/molecular spacers [14], through experiments [15, 16] and thanks to a theoretical foundation that originates from molecular electronics [17, 18].

On a general level, it is always possible to improve the performance of a spintronic device if the spin polarization P that underscores its properties is enhanced. At this time, within the spintronics of semiconducting spacers, three directions have been investigated. (a) One

involves using a ferromagnetic insulator (FI) as the dielectric spacer: the resulting tunnel barrier is then of different height for spin ↑ and ↓ electrons, resulting in a FM/FI/metal device with a spintronic response. Such devices have been shown to work, for example with EuS [19, 20], $La_xBi_{1-x}MnO_3$ [21–23], $CoFe_2O_4/MgAl_2O_4$ [24] or $NiFe_2O_4$ [25, 26] barriers. (b) Another approach is to select judiciously a FM/I pair such that the combination of band structure properties of the FM and I contribute to a large effective P. In the well-researched example of the Fe/MgO(001) system [27–29] and derivatives [30, 31], the MgO(001) ultrathin barrier's energy gap is defined by Δ_1 bands, and therefore allows electrons with Δ_1 electronic symmetry to tunnel across more predominantly than other symmetries [32, 33]. Since Fe(001) exhibits Δ_1 conduction at the Fermi level for spin ↑ but not spin ↓ electrons, the transport of a $\Delta_1^{\uparrow}$ electron across a Fe/MgO/Fe(001) MTJ in the antiparallel alignment of FM magnetizations is greatly hindered by the absence of available $\Delta_1^{\downarrow}$ states to tunnel into. The large resulting tunnelling magnetoresistance (TMR) at low bias then leads, through the Jullière model [34] (see equation (2)), to a large effective P. This P reflects the spin polarization of the carriers with Δ_1 symmetry present in Fe(001) as filtered by the MgO(001) barrier and detected by the Fe(001) counter-electrode. (c) As the focus of this special issue of *Journal of Physics: Condensed Matter*, the third direction is to use *half-metals* which, in an extensive definition that pertains to the material in bulk form, exhibit occupied states at the Fermi level with only one direction of electron spin, as originally predicted by de Groot *et al* [35] in 1983.

Half-metallic systems generically derive their properties from a delicate interplay of chemical order in epitaxial systems that may lead, through cooperative electronic effects, to the desired half-metallic property. Much research has gone into the elaboration and characterization of this tantalizing class of materials. Yet, do such materials exhibit half-metallic behaviour experimentally? Furthermore, when it comes to revealing the field of spintronics, are half-metals simply demonstrators of a physics that has already been observed by using other ferromagnets, or have half-metals fundamentally advanced our understanding of spintronics?

As we will discuss in this review of manganite thin films *with experimentally determined interfacial half-metallic properties*, it is in fact possible to reveal insights into spin-polarized solid-state tunnelling (Sp-SST) through a combination of the concepts present in the above spintronic directions of (b) symmetry filtering and (c) half-metals. The outline of this review is as follows. In addition to describing the electronic properties of manganites, section 2 will present a rapid overview of progress in spintronics research on manganite thin films and their use to demonstrate existing spintronic concepts. Section 3 will sketch the debate on the existence of the materials class of half-metals, and discuss how manganite interfaces with insulators may retain half-metallic properties, focusing on the $La_{2/3}Sr_{1/3}MnO_3$ (LSMO) manganite at the interface with $SrTiO_3$ (STO). Section 4 will present our results on the structural and electronic properties of LSMO/STO interfaces in MTJ stacks. Section 5 will then present our evidence, accrued through Sp-SST transport experiments, on the half-metallic property of LSMO in thin film form *at the interface* with STO. Our experiments show how this interfacial property is maintained despite the possible degradation in its spintronic performance due to inelastic transport processes at a finite applied bias. Finally, section 6 will present experiments wherein manganites are used to advance the field of spintronics.

2. Spintronic effects in manganite-based systems

After quickly describing the tight interplay between structure and exchange interactions that leads to the rich electronic properties in manganites, this section will summarize the implementations of spintronic devices that integrate manganites, and point the reader to more extensive, historical surveys of the field.

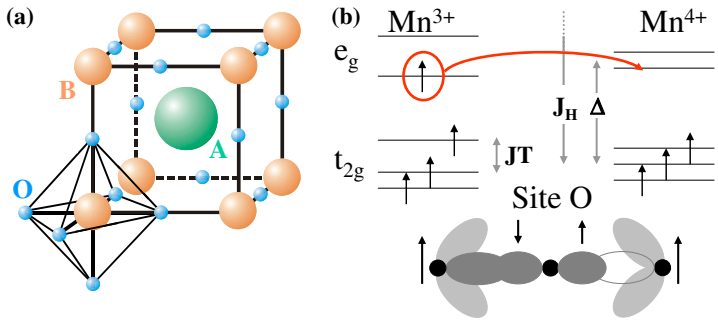

Figure 1. (a) Perovskite structure ABO_3 showing the O octahedra around the B site. (b) Schematic of the double exchange mechanism in $La_{2/3}Sr_{1/3}MnO_3$ between the σ orbitals of Mn^{3+} and Mn^{4+} sites across the oxygen 2p orbitals. For Mn^{3+}, the lifting of degeneracy between the two e_g levels, and between the top two t_{2g} levels, reflects the Jahn–Teller (JT) distortion of the oxygen octahedra around this site.

Manganites crystallize in the perovskite structure ABO_3, which is represented in figure 1(a). To illustrate the electronic properties of ferromagnetic manganites, we will focus here on the example of $La_{2/3}Sr_{1/3}MnO_3$. Its parent compound $LaMnO_3$ is antiferromagnetic. Upon replacing the trivalent La cation with a divalent cation such as Sr, the Mn sites must then assume a mixed 3+/4+ valence so as to conserve electro-neutrality. Referring to figure 1(b), the crystal field splitting $\Delta \sim 1.5$ eV is lower than the exchange energy $J_H \sim 2$ eV [36] so that, on a Mn^{3+} site, three electrons occupy the three $t_{2g} \uparrow$ levels, and the remaining electron lies on the first $e_g \uparrow$ level. The introduction of Mn^{4+} thus represents a form of hole doping of the e_g subband. Then, the double exchange mechanism, proposed by Zener [37] and extended by Goodenough [38–40], Anderson and Hasegawa [41], and Kubo and Ohata [42], takes place between Mn mixed-valence sites across O and contributes to the effective delocalization of this $e_g \uparrow$ electron among all Mn sites. These exchange interactions require that the initial and final states be degenerate in energy. This implies an identical spin referential on each Mn site, which is pinned by the three localized t_{2g} electrons. This spin-conserving process of electron transfer thus ensures long-range ferromagnetism, and the conduction of e_g electrons with spin $\uparrow$.

The lifting of degeneracy between a double exchange interaction across a pair of sites, and the same interaction in reverse, has been understood since 1995 [43, 44] as resulting from the Jahn–Teller (JT) [45] distortion on the Mn^{3+} site (see figure 1(b)). This effect in metallic manganites is now best understood as leading to transport through elastic JT polarons [46]. This cooperative form of transport of $e_g^{\uparrow}$ states can be hindered by many effects, including Anderson localization and deviations in the Mn–O–Mn bond angle that reduce the e_g bandwidth. Furthermore, the tendency for phase segregation to occur naturally in these mixed-valence manganites is also well documented (see, e.g. [47, 48]). It is this microscopic mechanism that is now understood to complement [48, 49] the double exchange model and JT effects in explaining the colossal magnetoresistance effect in manganites [50]. Finally, one must take into account coupling between electrons and magnons [51] or phonons [52] in such correlated electron systems.

The complex interplay between structural, magnetic and transport properties of manganites has galvanized efforts to tune the properties of these materials externally, through a local electric field [53–55] or by using ferrolectric materials [56, 57]. Such effects are reviewed in [58]. For technological purposes such as the synthesis of rectifying p–n junctions, several groups have worked on *electron*-doped manganites [59–61]. The control over the magnetic

properties of manganite nanodots [62] through substrate orientation, film thickness, island size, and island shape was also demonstrated [63].

Following in the footsteps of spintronics as described by transition metal ferromagnets and metallic spacers, IEC oscillations [1] have also been evidenced between manganite layers separated by the metallic spacer $LaNiO_3$ [64, 65]. The phenomenological damped RKKY model that was used to reproduce the experimental data was recently bolstered by an extended e_g model [66]. IEC experiments on $La_{2/3}Sr_{1/3}MnO_3/SrTiO_3$ multilayers have also been reported [67, 68].

Experiments and theory to describe the magnetization reversal due to the spin torque exerted by a spin-polarized current have in the past five years [69] represented a dynamic, expanding field with interfaces into spin dynamics. In this vein, some experiments have described how such mechanisms operate in manganites, both across pillars in the early work of Sun *et al* [70] and more recently in lateral constrictions [71–73]. A study of optically induced magnetization precession was recently reported [74].

Sp-SST experiments between manganite electrodes were first performed by Sun *et al* [75]. The LSMO/STO/LSMO MTJ system was the focus of many research efforts, with junctions from the IBM group [76] and UMP CNRS/Thales [77] yielding 500% TMR in 1997. Beautiful experiments were reported by the Blamire group on the coherent rotation of $La_{0.7}Ca_{0.3}MnO_3$ electrode magnetization in junctions comprising a $NdGaO_3$ tunnel barrier [78, 79].

Since this section is merely intended to be informative yet not exhaustive, we cannot fully describe the interplay of spintronic physics that underscores and links together all the above phenomena. The interested reader may refer to existing reviews on spintronics [80–85]. Furthermore, the reader may refer to the following reviews for more in-depth information regarding, and for insight into the historical progress of, research on manganites. In the voluminous review on 'metal–insulator transitions', Imada *et al* discuss the rich physics that are described by the materials class of perovskites [86]. Near the turn of the millenium, several reviews by Coey, Viret and von Molnár, and by Tokura and Tomioka focused exclusively and extensively on the class of mixed-valence manganites [36] with CMR properties [87]. More recent reviews by Ziese in 2002 [88], by Haghiri-Gosnet and Renard in 2003 [89], and by Dörr in 2006 [49] offer refinements in our understanding of the physics of manganites. As these reviews show, manganites are not simply studied on the basis of their properties, but are also used as tools to reveal the rich physics of spintronics. We will emphasize this aspect of manganite research in section 6.

3. Half-metallicity in bulk systems and at interfaces: the favourable case of the LSMO/STO interface

As this special issue reveals, there exists a controversy regarding the very existence of half-metals as a class of materials. This controversy essentially revolves around the definition of half-metallicity that is used. Where possible, we address the debate from our experimental perspective of the Sp-SST technique, and point the reader to the relevant portions of this review.

Much theoretical effort has focused on the impossibility of obtaining a *bulk* material with states at the Fermi level with one spin (hereafter called majority states for clarity), without states with opposite spin as well (hereafter called minority states for clarity). In a bulk framework, Nadgorny and co-workers introduced the interesting subtlety of distinguishing between half-metals and *transport* half-metals [90]. The former exhibit no minority states at the Fermi level in the half-metallic gap, while the latter does, yet these minority electron states do not contribute to conduction at E_F due to a much lower mobility relative to majority electron states. We note that the 94% value of *bulk* spin polarization that was obtained by Nadgorny and co-workers is

remarkable, since it was obtained despite the possible alteration of electronic properties through the possible chemical contamination and mechanical degradation of crystal structure that is inherent to the point-contact Andreev reflection technique (see the following contribution by this group). As we discuss in section 5.1, Sp-SST essentially probes all electron states at the LSMO/STO tunnelling interfaces, regardless of their mobility.

These minority states can appear at and near E_F in half-metallic candidate systems due to several mechanisms. (a) The mobility edge at the bottom of the t_{2g} antibonding band with minority character defines a minority electron energy gap relative to E_F. Localized electron states with the same electronic symmetry may appear below this band edge due to Anderson localization or bandwidth contraction [91].

Other mechanisms can lead to the presence of minority states with the same electronic symmetry as those of the majority band. (b) A finite temperature (FT) can intrinsically lead to a mixing of spin states [92–94]. (c) Starting from a purely half-metallic DOS at E_F, spin–orbit (SO) coupling may introduce off-diagonal components within a spin-resolved Hamiltonian, leading to a mixing of the pure spin states [95]. (d) In a one-particle framework of half-metals, minority electron states at and near E_F are forbidden. However, when taking into account electron correlation effects, such states can effectively appear due to a coupling between majority spin electrons and magnons into a non-quasiparticle (NQP) state [96–98].

Regarding the LSMO/STO interface, we discuss in section 5.3.2 the experimental manifestation of spin waves as indirect evidence for minority states at E_F, and in section 5.4 the electronic character of such minority states in relation to the above possible descriptions: localized $t_{2g}^{\downarrow}$ states, or $e_g^{\downarrow}$ states due to the FT, SO or NQP mechanisms.

For fundamental but also experimental reasons, much work has focused on characterizing the half-metallic property of suitable systems at specific or engineered interfaces with inorganic semiconductors [99–102]. Aside from the symmetry breaking that occurs for the half-metallic system, a key issue is the verification that no interface states exist and thus destroy the half-metallic phase [103].

Regarding manganite surfaces and interfaces, these efforts reflect an increasing focus on understanding the incidence of charge distribution on the electronic properties as evidenced by recent experiments [104–107]. It then becomes crucial to distinguish, in the case of an LSMO/STO interface, between a $MnO_2/La_{2/3}Sr_{1/3}O/TiO_2$ stacking of atomic planes (hereafter called a TiO_2 interface) and an MnO_2/SrO interface (hereafter called SrO interface).

Admittedly, the Sr doping that leads to the Mn mixed valence, and thus to ferromagnetism and half-metallic behaviour in manganites, results in a complex correlated electron system to model theoretically. Initial reports explain how the loss of cubic symmetry at a surface weakened the double exchange mechanism, leading to localization [91]. However, recent calculations from the Temmerman group emphasize the importance of the Mn^{3+} valence state, and its associated JT distortion, toward obtaining the half-metallic ground state in this manganite [108]. Furthermore, the ferromagnetic coupling between the LSMO bulk and the MnO_2 plane that is closest to the LSMO surface or LSMO interface with STO is strengthened in the case of electron doping (e.g. the TiO_2 interface of LSMO/STO) and weakened in the case of hole doping (e.g. the MnO_2 interface of LSMO/STO) [102, 109]. An SrO-type interface may recover strong ferromagnetic coupling to the bulk through the insertion of $LaMnO_3$ planes [102]. This is in apparent agreement with recent experiments that reveal the nanoscale suppression of magnetization at the LSMO/STO interface and a recovery with LMO insertion at the interface, if those experiments indeed involved an SrO interface [110] (see this group's contribution to the special issue). As we discuss in section 4, the LSMO/STO interfaces in our junctions are of TiO_2 type with electron doping due to a Mn^{3+}-rich phase. As hinted by Nadgorny *et al* back in 2001 [90], such charge transfer at a $La_{2/3}Sr_{1/3}MnO_3$ surface or

$La_{2/3}Sr_{1/3}MnO_3/SrTiO_3$ interface, and the JT distortion present on the Mn^{3+} site, have been calculated in a self-interaction corrected local spin density formalism to promote a half-metallic ground state [102, 109]. We note that this formalism does not currently take into account possible corrections (for instance, within a dynamical mean-field theory framework [111]) to the half-metallic ground state found for the LSMO/STO interface of type TiO_2, due to thermal effects, spin–orbit coupling or NQP states (see above).

4. Structural and electronic properties of the LSMO/STO interfaces in magnetic tunnel junction stacks

We now focus on manganite heterostructures that were grown at UMP CNRS/Thales, more precisely those composed of $La_{2/3}Sr_{1/3}MnO_3$ and $SrTiO_3$ films that were studied most extensively. $La_{2/3}Sr_{1/3}MnO_3$ was chosen because, for this doping concentration, this system exhibits the largest Curie temperature and the largest one-electron bandwidth [86] of all manganites, which results from a minimization in this system of all possible electronic disruptions to these figures of merit. The Fermi surface of (nearly) cubic $La_{2/3}Sr_{1/3}MnO_3$ exhibits Fermi surface nesting for the hole cuboid as well as for the electron spheroid, as predicted from calculations [112] and experimentally confirmed by Livesay *et al* [113]. As expected of a perovskite, deviations in oxygen stoichiometry have been shown to shift the Fermi level [114]. Park *et al* stimulated much research on $La_{2/3}Sr_{1/3}MnO_3$, with their spin-polarized photoemission results showing that the LSMO surface exhibited half-metallic properties, within the limits of this technique and experimental methodology [115, 116]. This section presents a compendium of results on structural and electronic characterizations of our LSMO and LSMO/STO/LSMO heterostructures, as a prelude to the Sp-SST experiments presented in section 5.

The LSMO/STO/LSMO trilayer heterostructures were grown on STO(001) substrates at 700 °C in a 350 mTorr molecular oxygen ambient by pulsed laser deposition (PLD) [117]. This large oxygen partial pressure ensures the oxygen stoichiometry of our LSMO thin films. Commercial STO(001) substrates were used with no particular treatment to obtain a particular atomic termination [106]. Additional details on growth conditions may be found in [77, 118].

The pioneering work of Viret *et al* in 1997 on the observation of TMR values reaching 550% in LSMO/STO/LSMO MTJs [77] led to much characterization groundwork to better understand the electronic properties of the LSMO/STO interfaces. Such LSMO/STO/LSMO stacks have been investigated extensively by transmission electron microscopy (TEM) [118–123]. Figure 2 presents a representative cross-sectional TEM picture of a LSMO/STO/LSMO trilayer stack. While the deposition conditions were identical to those used to grow trilayer stacks for MTJ experiments, the STO layer thickness was increased to 5.5 nm in order to increase the spatial separation between the top and bottom LSMO/STO interfaces with a view to electron energy loss spectroscopy (EELS) experiments that are discussed hereafter.

The perovskite $SrTiO_3$ consists of alternating TiO_2 and SrO planes, and the perovskite $La_{2/3}Sr_{1/3}MnO_3$ of MnO_2 (light) and $La_{2/3}Sr_{2/3}O$ (dark) planes. The cell height corresponds to the bulk 3.905 Å of $SrTiO_3$. Our structural investigations have not revealed the presence of stacking faults due to not controlling the atomic termination of either the substrate or the LSMO and STO layers. With a 0.83% in-plane lattice mismatch between LSMO(001) and STO(001), the trilayer grows epitaxially constrained on the STO substrate for LSMO thicknesses below ∼150 nm [123]. Strained LSMO films initially grow tetragonally on STO substrates, but the LSMO unit cell mostly recovers its rhombohedral distortion (pseudo-cubic with a 90.26°) at a thickness of 30 nm through twinning and with no dislocations [119, 120, 123]. Furthermore,

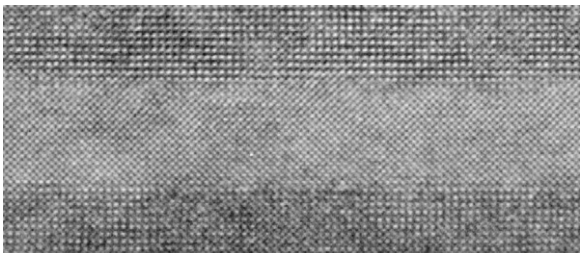

Figure 2. HRTEM of a 5.5 nm-thick STO layer sandwiched between LSMO layers in this fully epitaxially constrained heterostructure. MnO columns within LSMO, which exhibit bright contrast, are separated by the 3.905 Å STO lattice spacing of the substrate. The growth direction is from bottom to top. Adapted with permission from Maurice *et al* [106]. © (2006) Taylor and Francis.

magnetic measurements reveal Curie temperatures and magnetic moments that are very close to the bulk values for layers with a thickness 30 nm $< d <$ 150 nm [121]. We note that all transport measurements described in section 5 were performed on structures with a lower(upper) LSMO electrode that was 35(10) nm thick. While x-ray photoelectron spectroscopy studies of our samples reveal the formation during growth of a Sr-rich surface layer [124], this Sr-rich LSMO surface does not appear at the LSMO/STO interface.

Disruptions to the conventional Mn environment at a LSMO/STO interface can lead to the possible degradation in efficiency of the cooperative transport processes of double exchange and the JT effect. To probe further the structural and electronic properties of both LSMO/STO interfaces, such samples have undergone extensive EELS measurement campaigns at $T = 300$ K [122, 123] that have led to a clarified description of the LSMO/STO interfacial electronic properties, as reported recently [106]. We summarize here the main findings of this lengthy study by presenting results obtained on the sample shown in figure 2.

As described in section 2, the double exchange mechanism that leads to ferromagnetism and presumed half-metallic transport hinges on the valence state of Mn. Figure 3(a) presents the evolution of the Mn $L_{2,3}$-edge as the lower interface is crossed. When going from the bulk of the LSMO film to the interface, a chemical shift of the Mn-$L_{2,3}$ edge toward lower energies is observed, implying that the MnO_2 planes near the interface are *electron-doped* [106]. This occurs at both interfaces in our LSMO/STO/LSMO stacks. We note that, in the quite stimulating study of Yamada *et al* [104], the other SrO-type interface was found to lead to hole doping.

A number of explanations that can account for this alteration in electronic properties have been investigated. (1) A modification of the La/Sr ratio at the interface (implying a segregation of La and Sr cations) was discarded since the evolution of the ratio across the trilayer closely follows that of the Mn concentration. (2) A deviation in nominal oxygen concentration at the LSMO/STO interfaces could result in this electron doping. This hypothesis may be tested directly by examining the O-K spectra (see figure 3(b)), or indirectly through the associated transition metal L lines. However, the O-K edge spectra taken at both interfaces are in excellent agreement and, furthermore, are statistically a linear combination of bulk LSMO and bulk STO signals, with no new, additional interfacial signal [106, 122]. A comparison with other reference O-K spectra shows no evidence of oxygen vacancies, while the analysis of the Ti-$L_{2,3}$ edges reveals no valence change at either interface. (3) The electron doping of the MnO_2 interfacial planes could be a signature of a change in the Mn^{3+}/Mn^{4+} mixed-valence ratio at the interface. A careful examination and analysis of the Mn-$L_{2,3}$ peak shifts, and their splitting as the interface is crossed, reveals that this is indeed possible. This analysis is also consistent with a possible

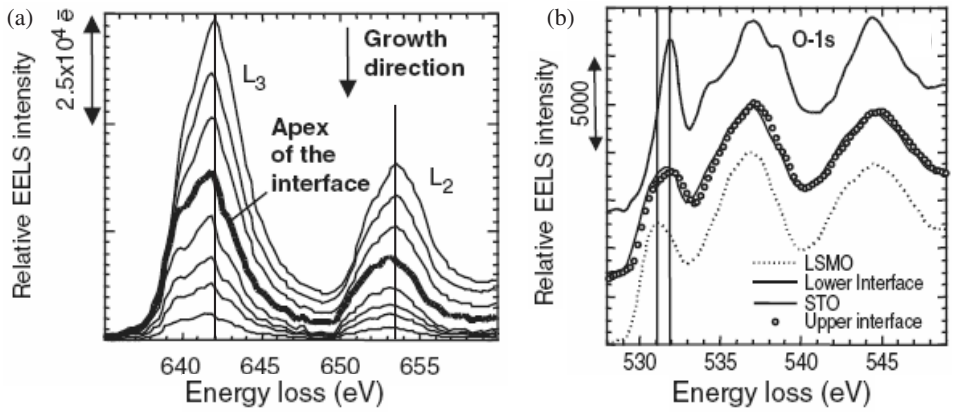

Figure 3. LSMO/STO/LSMO: variation of electron energy loss fine structure across the perovskite stack shown in figure 2, using the spectrum-line technique, at (a) the Mn-2p and (b) O-1s edges. The vertical lines in panel (a) are guides to the eye on the energy shift of the Mn-$L_{2,3}$ edges at the interface relative to those further into the LSMO bulk. Reprinted with permission from [106]. © (2006) Taylor and Francis.

JT splitting at the interface, since it would consist of more Mn^{3+} sites that are susceptible to this distortion.

In summary, EELS experiments have shown that the top and bottom interfaces in a LSMO/STO/LSMO epitaxial stack are quite similar and show no oxygen substoichiometry. Our structural investigations reveal no dislocations. Importantly, both interfaces exhibit an effective electron doping of the MnO_2 interfacial planes relative to the manganite bulk. This implies several salient points. (a) Both interfaces are of TiO_2 type—a surprising yet previously observed conversion of the terminating atomic plane of a perovskite ultrathin film that typically grows in unit cell layers [125]. (b) A transfer of electrons has occurred from the TiO_2 plane of STO toward the buried MnO_2 plane of LSMO. This therefore leads to (c) the possibility of a JT distortion at the interface due to the increased concentration of Mn^{3+} interfacial sites. Such charge transfer at a LSMO surface or LSMO/STO interface, and the JT distortion present on the Mn^{3+} site, have been calculated to promote a half-metallic ground state [102, 109] (see section 3). Both the half-metallic character of, and the possible JT distortion at, the LSMO/STO interface are evidenced by the transport experiments reviewed in the next section.

5. Spin-polarized tunnelling as a probe of the half-metallic property of TiO_2-type LSMO/STO interfaces

The previous section presented a review of the structural and electronic properties of LSMO/STO/LSMO stacks. In this section we present a compendium of spin-polarized tunnelling transport experiments on magnetic tunnel junctions that were prepared using these stacks. This section will focus on evidence for the half-metallic property of the LSMO/STO interface.

5.1. What to expect from the experimental Sp-SST technique and overview of results

Before presenting our results, it is important to frame our experimental technique of Sp-SST from/to LSMO/STO interfaces within the debate on half-metals. We discuss how, in determining the amplitude of spin polarization, our technique (a) probes the properties of a half-

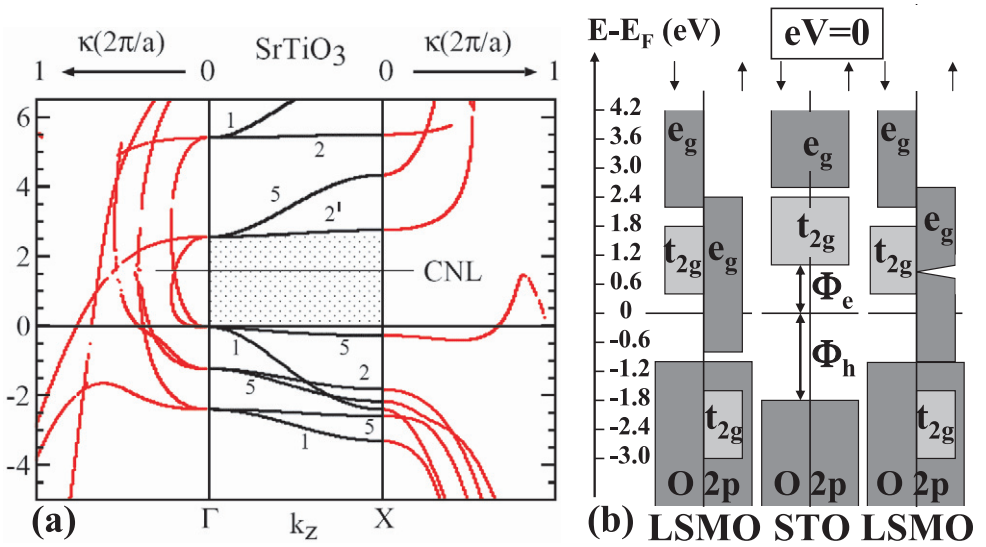

Figure 4. (a) Complex band structures of $SrTiO_3$ along [001]. Numbers indicate the Δ symmetries (e.g. $1 = \Delta_1$). The CNL is the charge neutrality level. From [7, 126]. (b) Schematic of the electronic symmetry-resolved DOS of STO(001) and the LSMO/STO(001) interfaces in a MTJ. Here $\Delta_{2',5}$ is t_{2g} and Δ_1 is (e_g, O 2p). This diagram omits the minute number of possible e_g minority states at E_F. From [7, 116, 127–130]. Adapted with permission from Bowen *et al* [7]. © (2006) American Physical Society.

metallic interface and not a transport half-metal [90]; and (b) is, due to an electronic symmetry mismatch effect [7], not biased by symmetry filtering considerations or by the LSMO band structure.

(a) Mazin suggested that the spin-polarized current across a tunnel junction be weighted by the electron mobilities in each spin channel [131]. Due to the exponential dependence of the tunnelling effect on distance, this transport process across a junction will involve, through the electric field developed across the dielectric, the injection of all interfacial states, whether within the conduction channels of bulk LSMO or poorly mobile yet present at the interface. We are therefore not in the scenario of characterizing a transport half-metal as described by Nadgorny *et al* [90]. This also means that we are testing the half-metallic property of the manganite *at an interface*. In simple terms, our Sp-SST technique is sensitive, for a vanishing applied bias, to localized states at both interfaces, because the lifetime of the localized electron/hole that should couple to bulk propagating states is shorter than the tunnelling lifetime for a thick barrier [132]. At finite bias, the Sp-SST technique's sensitivity to localized states at the collecting interface may decrease.

(b) As we will see hereafter through our Sp-SST technique, the spin polarization of a current at E_F in one MTJ interface is detected *after tunnelling across the barrier* by the spin-polarized states at the other interface. We emphasize that our method for determining the spin polarization P is not biased due to symmetry-filtering effects of the STO barrier (such effects account for the large effective spin polarization of, e.g., the bcc Fe/MgO(001) interface in MTJs; see e.g. [32]). Indeed, according to the complex band structure [133] of STO shown in figure 4(a), $SrTiO_3$(001) is a semiconductor with a direct band gap at the Γ point that spans 3.2 eV experimentally [134]. The charge neutrality level (CNL) is higher in energy than the mid-gap point, while the position of the chemical potential for intrinsic STO is quite close to

the bottom of the conduction band [128, 129]. The Fermi level at the LSMO/STO interface will thus lie within an energy range bounded by the intrinsic chemical potential and the CNL, depending on the latter's pinning strength [135]. This means that the interfacial Fermi level lies above the CNL, implying that t_{2g} electrons couple to the lowest tunnelling decay constant. The tunnelling process for the highly spin-polarized e_g electrons of LSMO will therefore not be helped by any symmetry filtering effect. On the contrary, symmetry filtering here would exacerbate whatever (minority) t_{2g} states that are present at E_F. For bias values below the electron and hole barrier heights, it is possible that, in addition to the Γ point, other Δ_1 states along Γ–M may be revealed through our Sp-SST technique across $SrTiO_3$ [136]. Yet, according to band structure calculations of $La_{2/3}Sr_{1/3}MnO_3$ (see e.g. [113]), both the Γ–X direction of electron transport and the Γ–M directions of STO tunnelling transmission effectively involve k-space at and around the Γ point, and thus the possible LSMO minority states that can appear at E_F depending on the theoretical formalism and the system under study (see section 3). Our technique is therefore probing precisely the problematic point in the LSMO band structure where deviations from half-metallic behaviour could occur.

Figure 4(b) presents a schematic that summarizes the overarching conclusions that are drawn from the work in this section on LSMO/STO/LSMO MTJs. The spin polarization of LSMO at the interface with STO was measured at low bias to reach 95%, and up to 99% through measurements at large bias. The difference essentially reflects the degradation of the observed P due to spin wave excitations at low bias, which do not contribute significantly at larger bias. We have evidenced the half-metallic minority gap of the LSMO/STO interface, $\delta = 0.34$ eV, that separates the Fermi level and the bottom of the minority band with t_{2g} symmetry, in quantitative agreement with inverse photoemission experiments. Finally, supposing that the 1% deviation from ideal half-metallicity at E_F is experimentally relevant[8], investigations at larger applied bias values reveal that any minority spin states at E_F cannot be of t_{2g} symmetry (despite the possible enhancement due to symmetry filtering), but could be of e_g symmetry and therefore described within the FT, SO or NQP pictures. In the following, after describing our experimental techniques, we will present our results on evaluating the spin polarization of the LSMO/STO(001) interface, and then provide an experimentally deduced description of the spin-polarized electronic properties of the LSMO/STO interface at and near the Fermi level.

5.2. On the synthesis and transport measurements of $La_{2/3}Sr_{1/3}MnO_3$*-based magnetic tunnel junctions*

To perform spin-dependent transport measurements across fully epitaxial LSMO/STO(7 ML)/LSMO(001) trilayers requires a robust antiparallel alignment of the LSMO electrodes' magnetization over a suitable external field range to be obtained. To achieve these magnetic properties, a Co(125 Å)/CoO(25 Å)/Au(150 Å) bilayer was sputter-deposited atop the PLD-grown oxide trilayer after brief exposure to air. We thus take advantage of the exchange-coupled ferromagnetic Co and antiferromagnetic CoO (with a blocking temperature that varies between 150 and 220 K from sample to sample) to effectively increase the coercive field of the top LSMO layer through direct ferromagnetic coupling between the top LSMO and Co layers.

To pattern LSMO-based trilayer stacks into MTJs for transport measurements, standard ultraviolet (UV) photolithography processes [137] were refined to take into account the materials specificity of manganites. The process limits all forms of sample heating to no more than 110 °C so as to avoid any oxygen desorption in the LSMO films [138]. To define the mesa structures, we utilize a neutralized Ar dry etching process that is controlled thanks to a

[8] The representation of the LSMO DOS in the schematic of figure 4(b) neglects the 1% deviation from full spin polarization as an experimental artifact for simplicity here.

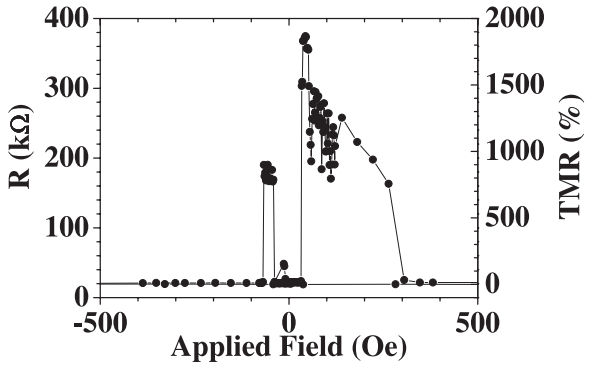

Figure 5. LSMO/STO/LSMO: magnetic field dependence of the resistance of a MTJ at $T = 4$ K. Adapted with permission from Bowen *et al* [139]. © (2003) American Institute of Physics.

secondary-ion mass spectrometer. Using this refined process typically yields working junctions with an area smaller than 32 μm^2 [139].

Direct current (dc) transport measurements were carried out in a four-point measurement configuration, with a positive sign of applied bias corresponding to electron injection toward the lower LSMO electrode. The resistance of the bottom LSMO electrode was always at least one order of magnitude smaller than that of the junction, so that an artificial enhancement of the spintronic response due to non-homogeneous current injection may be discounted [140].

5.3. Toward full experimental tunnelling spin polarization at finite temperature

Here we present evidence for a nearly total tunnelling spin polarization, first for a low value of applied bias where spin wave excitations dominate, and then at larger bias values for which this effect is attenuated.

5.3.1. Tunnelling spin polarization at low bias and overview of TMR/diff. TMR bias dependences. Figure 5 presents the magnetic field dependence of the resistance for a LSMO/STO/LSMO junction that was measured at $T = 4$ K at a dc bias voltage $V_{dc} = 1$ mV after field cooling. When sweeping the field from negative to positive values, the resistance of the junction rises from 19 to 375 kΩ, yielding through equation (2) a TMR ratio of 1850%. The asymmetry of the $R(H)$ loop reflects how the top LSMO layer is pinned through direct ferromagnetic coupling by the exchange-coupled Co/CoO overlayer. The noisy resistance signal in the AP MTJ configuration reflects poor micromagnetic control of the junction state over the junction surface area. This issue is attenuated at larger bias. Ishii *et al* have resolved this issue by doping one of their manganite electrodes with Ru [141], leading to a good antiparallel alignment for $T < 300$ K.

To relate the measured TMR to the LSMO/STO interface spin polarization P, we can use the Jullière model:

$$\mathrm{TMR} = \frac{I_P - I_{AP}}{I_{AP}} = \frac{R_{AP} - R_P}{R_P} = \frac{2P_{Inj}P_{Col}}{1 - P_{Inj}P_{Col}}, \tag{2}$$

which alternately relates the MTJ current I or the resistance R, in the parallel (P) or antiparallel (AP) alignments of electrode magnetizations, to the spin polarizations P at E_F of the MTJ interfaces that inject (P_{Inj}) and collect (P_{Col}) the current. In a worst-case scenario, we suppose that both interfaces have the same spin polarization, i.e. that $P = P_{Inj} = P_{Col}$. In this case,

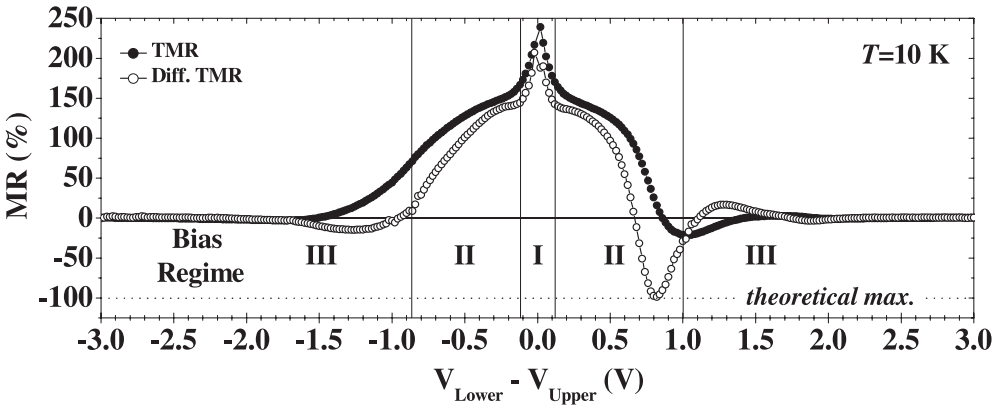

Figure 6. LSMO/STO/LSMO: bias dependence of TMR and diff. TMR at $T = 10$ K. Adapted with permission from Bowen *et al* [7, 127]. © (2005, 2006) American Physical Society.

using equation (2), the measurement of TMR $= 1850\%$ reflects a spin polarization $P \simeq 95\%$. Measurements at $T = 4$ K and $V_{dc} = 1$ mV on several other junctions yield a spin polarization no lower than 90%.

One may infer that the $P = 95\%$ represents a lower bound on the maximum spin polarization by considering the related incidence of (1) temperature and (2) applied dc bias on this TMR measurement. (1) As we have shown elsewhere [142], the TMR and inferred spin polarizations, when measured at low bias, decrease with increasing temperature. This most likely reflects the thermal onset of spin wave excitations that, in addition, can dominate transport at this *very low* value of applied bias. (2) Indeed, spin wave excitations may also occur within a low-bias regime around $V = 0$, leading to a dramatic reduction in TMR [127]. We will develop this second point in what follows. Taken together, these arguments suggest that ac measurements at $V_{dc} = 0$ should yield higher values of TMR and therefore of P.

To provide an overview of discussions in this section, it is most straightforward to present in figure 6 the extended bias dependence of TMR across a LSMO/STO/LSMO junction at $T = 10$ K. The bias asymmetry reflects slight differences between the two junction interfaces. We note that the 20 mV bias step used here does not reveal the large TMR at very low bias.

In order to reveal spin-polarized features at a given applied bias (i.e. energy away from E_F), the straightforward examination of TMR(V) is not necessarily useful since, as per equation (2), TMR $\sim I$ and as such represents an energy convolution of the DOS [143]. It can therefore be more appropriate to consider differential TMR (diff. TMR):

$$\text{diff. TMR}(V) = \frac{G_P(V) - G_{AP}(V)}{G_{AP}(V)} = \frac{2P_{Inj}(E_F)P_{Col}(E_F + eV)}{1 - P_{Inj}(E_F)P_{Col}(E_F + eV)}, \tag{3}$$

which, thus defined, takes on percentage values in the range $-100 <$ diff. TMR $< +\infty$. In equation (3), the derivation of the relationship between diff. TMR and $P_{Inj}(E_F)$ and $P_{Col}(E_F + eV)$ follows the same framework reported by Jullière [34] to relate TMR to $P_{Inj}(E_F)$ and $P_{Col}(E_F)$, but with no energy integration. Thus, diff. TMR can, for an applied bias V, therefore track DOS features at an energy eV away from E_F. In this sense, diff. TMR is more suitable for probing the spectroscopic response of a MTJ than TMR.

This bias dependence can be split into three regimes that are understood as follows: (I) a low-bias regime that is dominated by spin wave generation; (II) an intermediate bias regime that is dominated by DOS features of the electrode that collects the electron current; and (III) a regime for which the junction potential profile itself dominates. In what follows, we will present

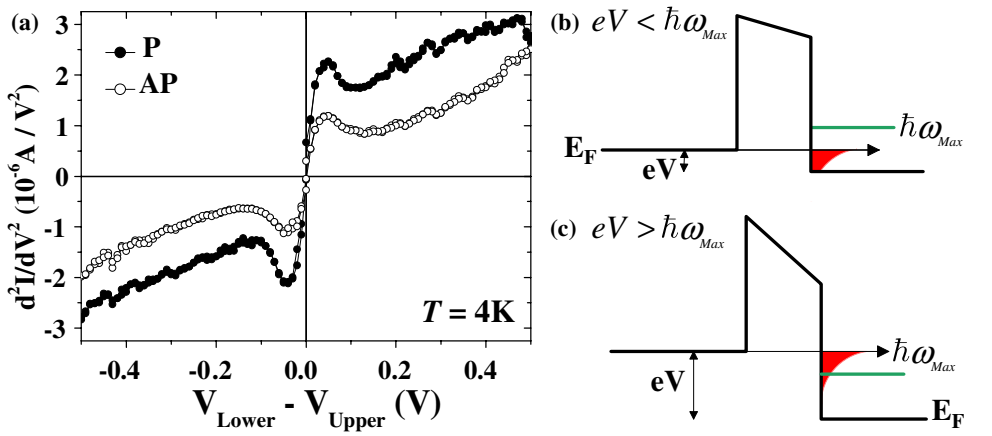

Figure 7. (a) LSMO/STO/LSMO: bias dependence of the second derivative of MTJ current in the P and AP junction configurations. From [145]. Schematics depicting (b) the low-bias regime dominated by magnon excitations and (c) the intermediate-bias regime for which the influence of magnon excitations on the total tunnelling current is lessened. The transition from one bias-dependent tunnelling regime to the other occurs at the energetic extent $\hbar\omega_{\mathrm{Max}}$ of the magnon excitation spectrum. The tunnelling transmission probability for energies below that of the injecting electrode's Fermi level is also indicated.

figures that focus on salient features of the bias-dependent spintronic response in these three regimes.

5.3.2. Bias regime I: spin wave excitations. In the low-bias regime I, a dramatic drop in TMR amplitude is observed. Within this bias range, junction conductance $G(V)$ exhibits a pronounced dip for $|V| \lesssim 120$ mV [127]. Such a zero-bias anomaly in $G(V)$ has been identified as the signature [144] of spin wave excitations. This inelastic effect naturally explains the large drop in TMR amplitude [144] within the bias regime I. We note that diff. TMR $\sim G$ naturally exhibits a clear cutoff between regimes I and II, while the TMR decrease lessens at larger bias due to energy convolution.

The signature of such spin wave excitations (and other inelastic transport phenomena) can be seen by examining the second derivative of $I(V)$ [146, 147]. As seen in figure 7(a), the antisymmetric response around zero bias, and the peak observed here at about 40 mV for both P and AP junction configurations, are characteristic of this inelastic tunnelling mechanism. The two bias regimes I around $V = 0$ essentially reflect the magnon generation spectrum with extent $\hbar\omega_{\mathrm{Max}} \sim 120$ meV. Within this energy range, hot electrons can thermalize through the emission of a magnon, as schematized in figure 7(b). Hot electrons with an energy that exceeds this range (see figure 7(c)) can no longer thermalize to E_{F} through the emission of a single magnon, and a two-magnon process is then more unlikely.

Beyond analytical models (see, e.g., [144]), the description of the role of inelastic processes on Sp-SST is only nascent. We note that magnons have been shown to alter dynamically the electronic structure of a material [148]. A fundamental *ab initio* approach to treating the incidence of phonons on a current [149] was proposed, and extended into an emerging *ab initio* theory that addresses the incidence on spin-polarized tunnelling transport of inelastic processes such as magnons or phonons [150, 151].

Spin wave excitations are explained in manganites as the coupling between ionic spin waves with the t_{2g} electronic character of the localized Mn spins, and electron spin density

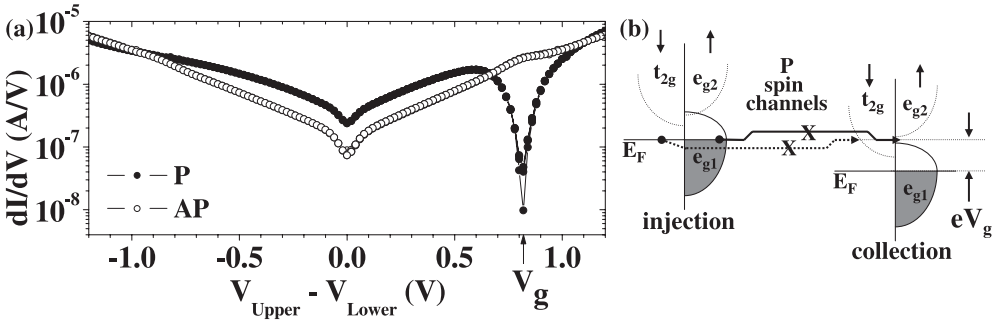

Figure 8. LSMO/STO/LSMO: (a) conductance $\mathrm{d}I/\mathrm{d}V$ versus applied bias in the parallel (P) and antiparallel (AP) junction configurations. (b) Schematic of the two interfacial densities of states for an applied bias $V_g = 0.82$ V. Arrows depict the two spin channels in the parallel (P) configuration, which are blocked (crosses). Adapted with permission from Bowen *et al* [154]. © (2005) Institute of Physics.

waves with the e_g electronic character of the conduction carriers. The resulting spin wave excitation is then a composite magnon [152]. This implies that minority states with both e_g and t_{2g} electronic character can in principle exist at E_F in LSMO. Anomalous single-magnon processes in half-metals have previously been evidenced in LSMO [153]. Interestingly, the possibility [51] of generating spin waves within this 120 meV energy range above E_F at the LSMO/STO interface can be interpreted in terms of the presence of minority states at E_F. Our experimental results in section 5.4 show that such states can only be of e_g character.

5.3.3. Bias regime II: probing half-metallicity in MTJs beyond the magnon excitation spectrum. While large bias values circumvent the incidence of magnon generation at the collecting interface, this condition alone is not sufficient to further address the question of the spin polarization from the *injecting* MTJ interface. In addition, one requires a highly spin-polarized feature in the energy-dependent DOS of the *collecting* MTJ interface. This would lead to a large diff. TMR that could then be interpreted in terms of spin polarization (see equation (3)).

In this vein, figure 8(a) presents the bias dependences of conductance, $G = \frac{\mathrm{d}I}{\mathrm{d}V}$, in the P and AP MTJ configurations. We recall that, in the P junction configuration, both spin ↑ and (if any) spin ↓ electrons at the LSMO Fermi level of the injecting electrode may tunnel into respective spin ↑ and ↓ empty states of the collecting electrode. In the AP configuration, the spin channels are crossed, such that injected spin ↑ electrons tunnel toward spin ↓ empty states and vice versa. The striking observation is that, past $V = 0.6$ V, while G_{AP} continues to increase, G_P decreases and reaches a minimum at $V_g = 0.82$ V, which is one order of magnitude lower than the conductance found at $V = 0$. As shown in figure 8(a), the several consecutive bias sweeps, which were performed for this dataset up to $V = \pm 3$ V, attest to the resilience of the effect observed.

This effect cannot result from spin-polarized states within the STO ultrathin barrier, since this would involve a similar dip in G_P at negative bias values. This was not observed experimentally (see figure 8(a) and [145]). On the other hand, our result could reflect the nearly total spin polarization of the LSMO/STO collecting interface at $E = E_F + eV_g$. It would nevertheless have to be probed by a nearly fully spin-polarized current originating from the Fermi level of the injecting LSMO/STO interface. Indeed, as schematized in figure 8(b) within a junction interfacial DOS framework, this absence of conduction in the P configuration at V_g implies that both spin channels are blocked. (i) P spin ↑ channel: initial spin ↑ electrons are available in LSMO for tunnelling, but at energy $E = E_F + eV_g$ no final spin ↑ states

are present to tunnel into. (ii) P spin ↓ channel: since spin ↓ final states are available at $E = E_F + eV_g$ [127], the blocking of this channel implies, within experimental limit, that no spin ↓ injecting states exist in LSMO at E_F. We now discuss the physics that describes the conduction G_P in each of these two spin channels.

(i) The absence of available spin ↑ states at $eV_g + E_F$ in the DOS of the LSMO/STO collecting interface effectively reflects the presence of a spin-polarized pseudogap at that energy. Presently, we cannot advance a fully supported explanation for the occurrence of this pseudogap. Nevertheless, this pseudogap could result from a JT distortion of the oxygen octahedral environment of Mn sites at the lower LSMO/STO interface. Such a distortion indeed leads to a pseudogap at broadly the correct energy above E_F, as calculated for bulk $La_{0.7}Ba_{0.3}MnO_3$ manganites [155]. This JT distortion scenario is supported by the EELS experimental results on our junction interfaces [106] (see section 4) and from theoretical work on the electronic properties of the LSMO surface and LSMO/STO interfaces [102, 109] (see section 3). We surmise that the JT distortion in these Sp-SST experiments is more significant at the lower interface than at the upper interface, so that the upper interface does not exhibit the full opening of a pseudogap (see figure 8(b)).

(ii) P spin ↓ channel: since spin ↓ final states are available at $E = E_F + eV_g$ [127], the blocking of this channel is the direct consequence of the very high spin polarization P_{Inj} at E_F of the injecting upper interface.

To characterize the amplitude of this spin polarization, we can evaluate quantitatively the extent to which both spin channels are blocked for $G_P(V_g)$. Indeed, diff. TMR reaches −99% at exactly V_g (compare figures 8 and 6)[9], i.e. within 1% of the theoretical maximum that defines fully half-metallic behaviour. Assuming that $P = P_{Inj}(E_F) = P_{Col}(E_F + V_g)$ leads to $P = 99\ \%$[10].

This value is constrained by certain experimental limitations. The most glaring is that our conductance measurement, $G = \frac{dI}{dV}$, is not dynamic. As seen in figure 8(b), the data that describes G_P is spiked. Thus, with more data points taken around V_g, it could have been possible to achieve an even lower conductance, and therefore larger values of diff. TMR and P. Furthermore, the dip in G_P strongly lessens with increasing temperature [145]. Measurements at lower temperature are therefore expected to yield even larger diff. TMR and P. In conclusion, within experimental limit, we state that, at V_g in the AP configuration, there is a fully spin-polarized tunnelling current from majority spin injecting states to minority spin collecting states. This implies that almost no injecting spin ↓ states, whether propagating or not, are present at the Fermi level of the LSMO/STO interface.

5.4. On the electronic character of any Fermi level minority states

In the preceeding section, we presented experimental evidence for a large spin polarization P at the Fermi level of the LSMO/STO interface, which can reach 99%. We argued there how experimental limitations in our techniques could imply that a value even closer to ideally full spin polarization may be achieved. In this section, we address the electronic nature of the spin ↓ states that could represent the 1% experimental deviation from ideal half-metallicity at the Fermi level of the LSMO/STO interface, if such a deviation is experimentally relevant. As discussed in what follows, our experiments on the bias response of LSMO/STO/LSMO junctions evidence the energy position above the Fermi level of the mobility edge of the minority t_{2g} band, and rule out the presence of any $t_{2g}^{\downarrow}$ states in the DOS at the Fermi level

[9] One sees that TMR (V_g) is not a noteworthy value. This supports the use of diff. TMR over TMR for spectroscopic studies of the counter-electrode DOS as well as of the tunnel barrier.

[10] Using the $P_{Inj}(E_F) = 95\%$ found at low bias leads to an unphysical value for $P_{Col}(E_F + eV_g)$. This could indirectly reflect the incidence of magnon generation on the value of P derived from the measurement at low bias.

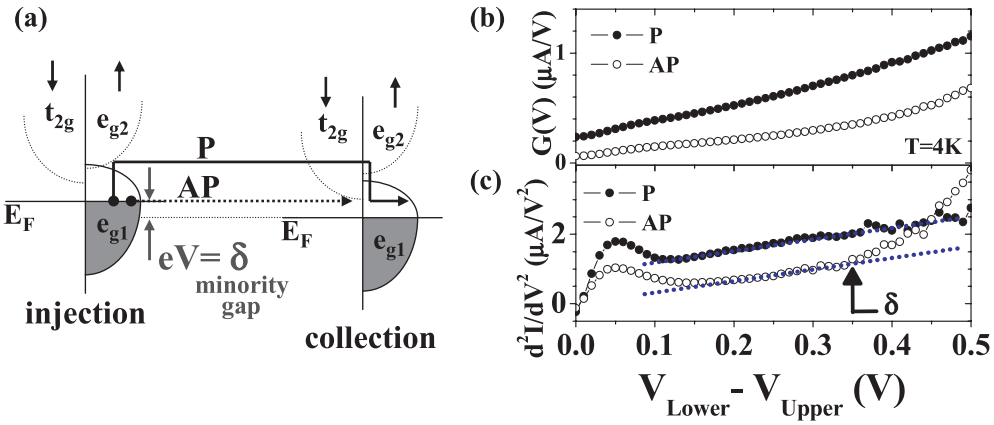

Figure 9. LSMO/STO/LSMO: (a) Schematic of the two spin channels that transmit the tunnelling current for an applied bias that spans the energetic extent of the LSMO/STO minority gap. (b) Junction conductances $\frac{dI}{dV}$ in the parallel (P) and antiparallel (AP) junction configurations. (c) Bias dependences of the derivative of the junction conductances in (b). Adapted with permission from Bowen *et al* [127]. © (2005) by the American Physical Society.

of the LSMO/STO interface, thereby eliminating one mechanism for a deviation from half-metallicity (see section 3).

5.4.1. Signature of the minority gap. Referring to figure 6, if one discards the sharp drop in TMR and diff. TMR present in the transport regime I and ascribed to the thermalization of hot electrons through magnon generation, the transport regime II above the zero bias anomaly of the transport regime I is characterized by what appears to be a plateau within the range 120 mV $\leqslant V \leqslant$ 300 mV that consists of a more slowly decreasing TMR as the applied bias is increased. As Bratkovsky pointed out [156], this behaviour may be expected of a MTJ with two half-metallic electrodes. Indeed, as schematized in figure 9(a), it is only when the applied bias allows electrons to tunnel from E_F into available states at the bottom of the minority band that the TMR should decrease from its maximum value. We have also found a fairly constant evolution of the spin asymmetry $\Delta I = \frac{I_P - I_{AP}}{I_P + I_{AP}} = P^2$ over the bias range defined by this plateau [127].

To pinpoint the energy onset of the minority t_{2g} band, we examine in figure 9(b) the junction conductances. As expected given the dominant presence of majority e_g states at E_F, $G_P > G_{AP}$. We observe that G_P, which reflects the spin $\uparrow$ tunnelling channel between the two half-metallic electrodes, increases linearly within the bias range 120 mV $< V <$ 600 mV. In contrast, G_{AP} departs from this progressive increase around $V \simeq 0.3$ V. To compare the differing behaviours of G_P and G_{AP} more quantitatively, we present the conductance derivatives in figure 9(c). As shown in the panel, it is possible to fit parallel lines across the $\frac{d^2I}{dV^2}$ data for both P and AP within the bias range 150 mV $\lesssim V \lesssim$ 350 mV, which implies the opening of the same additional conduction channels with increasing bias amplitude. However, $\frac{d^2I_{AP}}{dV^2}$ abruptly departs from this behaviour at a value of $V = 340$ mV, suggesting the presence for $E > E_F + 340$ meV of a strong increase in the spin $\downarrow$ DOS. This quantitatively reflects the onset of tunnelling into the bottom of the $t_{2g}^{\downarrow}$ band. This minority gap $\delta = 340$ meV has been corroborated by measurements at both interfaces of several MTJs to within an error of 40 meV. Our analysis and interpretation are bolstered by an experimental agreement [127] with the theory of Bratkovsky [156] regarding how G_{AP} ought to increase once the minority gap is exceeded. Within a picture of symmetry-coherent transport across the LSMO/STO/LSMO

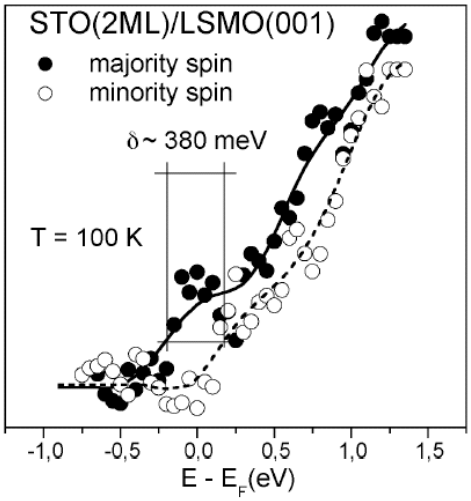

Figure 10. SPIPE spectra on a STO(001)//LSMO/STO(2ML) sample at $T = 100$ K for the spin ↑ (closed circles) and ↓ (open circles) channels. Adapted with permission from Bowen *et al* [127]. © (2005) by the American Physical Society.

MTJs, the ability for e_g electrons to probe empty t_{2g} states in the AP configuration, despite this symmetry mismatch, likely reflects a decoherence process, much as is argued in the Fe/MgO(001) system [32].

To confirm the spectroscopic character of our bias-dependent experiments and analysis of our LSMO/STO/LSMO MTJs, spin-polarized inverse photoemission (SPIPE) spectroscopy experiments were performed on a 35 nm LSMO thin film covered with two monolayers (2 ML) of STO. The experimental geometry at normal incidence with respect to the LSMO(001) surface thus yields spectroscopic data along the Γ–X direction in the first Brillouin zone. The SPIPE spectra taken at $T = 100$ K in an energy range close to E_F for a LSMO/STO bilayer are presented in figure 10. The two distinct lineshapes for majority and minority electrons clearly show that the sample is metallic for majority electrons and semiconducting for minority electrons. The shift between the onset of each spin signal pinpoints the minority gap between E_F and the bottom of the minority t_{2g} band at $\delta = 380 \pm 50$ meV. This value is similar that found for a LSMO surface [157], in good quantitative agreement with the value obtained through Sp-SST.

These experiments thus provide information on the energetic position of the minority gap in LSMO when at the interface with STO. Their importance in the field cannot be overstated, since the crossing of this band at and near the Γ point represents one scenario to describe the deviation in the LSMO system from half-metallic behaviour. Indeed, theoretical reports in the literature have pegged the minority gap δ within a range $0\ \text{eV} < \delta < 1.6\ \text{eV}$ [108, 113]. It should be noted here that our experimental results apply especially to LSMO at a TiO_2-type interface with STO, i.e. to a perovskite interface. We note that the Sp-SST technique was also used to evaluate quantitatively a half-metallic gap in Co_2MnSi-based junctions with an Al_2O_3 tunnel barrier [158, 159].

5.4.2. Discriminating between the e_g and t_{2g} nature of any minority states at E_F. If the 1% deviation from experimental half-metallicity at the LSMO/STO interface, rather than representing an experimental limitation or artifact, does indeed describe spin ↓ electron states at E_F, then several theories exist to describe the presence of such states.

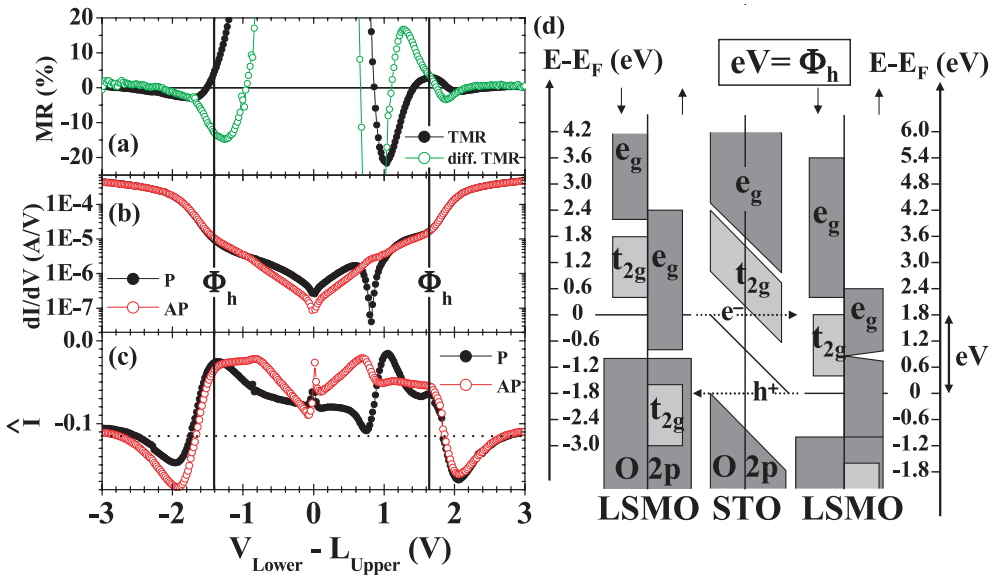

Figure 11. Bias dependences of: (a) TMR and diff. TMR, (b) differential conductance, and (c) $\hat{I}(10\ \mathrm{K}, 70\ \mathrm{K}) = [I(70\ \mathrm{K}) - I(10\ \mathrm{K})]/I(10\ \mathrm{K})$ in the parallel (P) and antiparallel (AP) junction configurations. (d) Schematic of the electronic symmetry-resolved DOS of STO(001) and the LSMO/STO(001) interfaces for $eV = \Phi_h$. This diagram omits the minute number of possible e_g minority states at E_F. From [7, 116, 127–130]. Adapted with permission from Bowen *et al* [7, 127] © (2005, 2006) by the American Physical Society.

In the preceeding section 5.4.1, we presented Sp-SST experiments that pinpointed the *mobility edge* of the minority t_{2g} band at 340 meV above E_F at the LSMO/STO interface. However, our Sp-SST technique (see section 5.1) and the analysis methodology of the preceeding section do not exclude the possible presence of localized states with t_{2g} electronic character below this minority band.

As explained in section 3, the FT and SO mechanisms can also effectively introduce minority spin states at E_F, but with e_g electronic character, while the NQP mechanism could lead to minority states with either e_g or t_{2g} character due to the possibility of composite magnons in manganites [152]. The methodology of the preceeding section 5.4.1 cannot address this possibility, since it used similar junction conductance increases in the P and AP configurations as a basis for the observation of the mobility edge of the $t_{2g}^{\downarrow}$ band.

The observation of (composite) spin waves at low bias due to the injection of e_g electrons (see section 5.3.2) suggests that any minority states be of t_{2g} or e_g nature [152], and respectively reflect localized or FT/SO states, as well as NQP states. We therefore suppose that, in addition to the large number of spin ↑ states at E_F with e_g electronic character, there also exist a few $e_g^{\downarrow}$ and $t_{2g}^{\downarrow}$ states. In group theory notation, this corresponds to $\Delta_{1,2}^{\uparrow}$ and $\Delta_{1,2,2',5}^{\downarrow}$ electronic symmetries. We can discard all Δ_2 states from the tunnelling current since, referring to figure 4(a), these will decay much more rapidly within the barrier[11].

We now discuss theoretical and experimental results [7] that can help us to focus on likely theoretical pictures to describe these few possible minority spin electron states at E_F. We present in figure 11 a set of panels that describe various aspects of the spin-polarized transport

[11] This argument is not detrimental to our conclusion since, to compare the two theoretical frameworks with experiment, we will consider e_g versus t_{2g} symmetries, not whether Δ_2 states are present or absent at E_F.

properties of the LSMO/STO/LSMO junction under an applied bias. Below a reproduction of the TMR(V) and diff. TMR(V) data of figure 6 are the bias dependences of junction conductances G_{P} and G_{AP}. We now focus on the transport regime III. Both G_{P} and G_{AP} exhibit a large increase past $V = 1.65$ V. At negative bias, this occurs at $V = -1.4$ V. This spin-independent conductance increase reflects exceeding the junction barrier height Φ, and is described as Fowler–Nordheim tunnelling [160]. In this transport regime, the electrons perceive a reduced barrier thickness, leading to the large increase in junction conductance. We confirm this interpretation by examining $\hat{I}(10\,\mathrm{K}, 70\,\mathrm{K}) = I[(T = 70\,\mathrm{K}) - I(T = 10\,\mathrm{K})]/I(T = 10\,\mathrm{K})$ (see figure 11(c)). Indeed, $\hat{I}$ exhibits a peak at the same bias value as well as a similar bias dependence above this value for both the P and AP configurations. Such peaks in $\hat{I}$ reflect the additional tunnelling current due to carriers injected at the barrier height with additional energy $k_{\mathrm{B}}T$ [161][12].

The 1.65 eV value of the barrier height is quite surprising, given the potential profile of the junction (see figure 4). Indeed, the bulk STO direct band gap is $E_{\mathrm{g}} = 3.2$ eV [134], and is reduced in ultrathin films [162]. Prior experiments to those presented in the figure reveal that $\Phi = 1.83$ eV [145][13]. Thus, here we observe experimentally that $\Phi > E_{\mathrm{g}}/2$. Since we have previously established that, across our LSMO/STO/LSMO junction, $\Phi_{\mathrm{e}} < \Phi_{\mathrm{h}}$ (see figure 4(b) and section 5.1), this implies that the barrier height observed here is the one for holes, which is defined as the energy difference between the interfacial E_{F} and the top of the STO valence band, i.e. $\Phi_{\mathrm{h}} = 1.65$ eV here.

Yet we also observe the same rate of conductance increase with no abrupt change for $eV < \Phi_{\mathrm{h}}$. This means that, once $eV > \Phi_{\mathrm{e}}$, the Δ_1 electrons that are injected from the Fermi level of the LSMO/STO interface *continue to tunnel* despite the presence of available $\Delta_{2',5}$ states in the conduction band of STO. It is only when the applied bias exceeds the barrier height defined by the STO valence band of O 2p character ($\Delta_{1,5}$) that the current enters the Fowler–Nordheim regime. To summarize these findings, figure 11(d) presents a simplified schematic of the symmetry- and spin-resolved potential profile across LSMO/STO/LSMO resulting from an applied bias $eV = \Phi_{\mathrm{h}}$. This potential profile at finite bias is correct at the Γ point for which the Fowler–Nordheim regime is operative across STO(001).

The implication of these results and analysis is that, if the current is not tunnelling with respect to the t_{2g} band (with $\Delta_{2',5}$ electronic symmetries), but rather to the O 2p band (with $\Delta_{1,5}$ electronic symmetries), then the injected current cannot at all consist of electrons with t_{2g} symmetry. While this is trivially the case regarding majority carriers with e_g symmetry, this demonstrates that any minority states must also be only of e_g symmetry. These experiments and analysis therefore do not support the picture of localized minority states at E_{F} that originate from the minority t_{2g} band.

6. Using manganites to reveal the field of spin electronics

We presented in section 2 a limited compendium of research on spintronic effects that are also observed in manganite systems after initial discovery in other systems. This section discusses the reverse research feedback of utilizing manganite materials to perform novel revelations of spin electronics.

The experiments of the preceeding section 5 have served, in that context, to underscore the experimental half-metallic nature of the LSMO/STO interface [139, 154]. Yet these experiments also affirm fundamental tenets of the Sp-SST technique. Indeed, these experiments showed that a current, injected from the Fermi level of a MTJ electrode, can, after tunnelling,

[12] The use of free-electron models in a low-bias approximation is inappropriate for this system.

[13] The barrier height reduction reflects an effect of junction state formation that is beyond the scope of this review and will be described elsewhere.

remain fully spin-polarized *at large bias* (see section 5.3.3), despite possible spin-flip relaxation mechanisms—an important result for spintronic applications. This experimentally confirmed property of Sp-SST, in turn, revealed the possibility of performing spin-polarized spectroscopy [127] using Sp-SST, in quantitative agreement with spin-polarized inverse photoemission spectroscopy (see section 5.4.1).

These LSMO/STO/LSMO experiments at larger bias [7] also described a novel scenario within the field of Sp-SST that takes into account the interplay of band structure throughout the epitaxial MTJ between the ferromagnetic electrodes and the tunnel barrier (see section 5.4.2), thereby hinting at a convergence within spintronics of GMR and TMR.

Symmetry filtering in the course of Sp-SST implies that all injected states tunnel across the semiconducting spacer with respect to the nearest band with the correct symmetry. In the LSMO/STO/LSMO case, we have shown how the FM injects only e_g states (Δ_1, Δ_2) that are 99% spin-polarized. Yet, contrary to the Fe/MgO(001) case, the nearest band here is the t_{2g} conduction band (with Δ_2' and Δ_5 symmetries), leading to our aforementioned observation that such e_g electrons continue to tunnel above the electron barrier height, despite the presence of available states within the spacer at that energy due to their mismatched t_{2g} symmetry. This result reveals that symmetry filtering in this Fowler–Nordheim tunnelling regime is *fully* operative here. An equivalent progress in the Fe/MgO(001)-type junctions would be the experimental observation of the 5000% TMR that were predicted [32, 33].

This case of a *symmetry mismatch* between injected states and the nearest band in the tunnel barrier represents an important opportunity to perform fundamental studies of Sp-SST. Indeed, we showed how this can lead to an experimental picture of *both electron and hole tunnelling* in the same device. This scenario is also useful to evaluate the tunnelling distance over which this mismatch, i.e. symmetry-based transport, remains operative. Finally, these manganite-based experiments show how it is possible to reduce leakage currents in a suitably designed epitaxial transistor by effectively increasing the band gap, a crucial result for technological applications. Some Fe(001)-based experiments have been proceeding in this direction with the integration of a Cr(001) spacer with no Δ_1 states at E_F [163, 164], though in that case the effect can be dominated by the presence of an interface state.

Tunnelling above barrier heights represents a hybrid GMR/TMR scenario that exemplifies the emerging convergence of these two fields of spintronics. Indeed, the potential landscape perceived by the charge carriers may correspond to the insertion of a metallic interlayer if the symmetry of the relevant band in the semiconductor spacer matches that of the injected carriers [7]. This scenario leads to oscillations in TMR and diff. TMR (see figures 6 and 11) that are due to the presence of quantum well states (QWS) within the spacer [7, 165].

The formation and detection of QWS through transport at finite bias should be accompanied by concurrent changes to IEC [166] as probed by transport. Thus far, IEC has been described and observed only at zero bias, notwithstanding the spin torque research on MTJs with a related but not identical theoretical framework [167, 168]. At a finite applied bias, this IEC should also reflect the potential landscape that charge carriers probe at that bias value. According to our experiments [145], the intermediate magnetic coupling between manganite interfaces and the bulk represents an ideal opportunity to probe such spintronic physics thanks to manganite systems, in the footsteps of early work on manganite IEC and GMR effects across metallic spacers [64–66]. These considerations appear in the transport regime III of Sp-SST above the electron barrier height (see figure 6), which is lowest here. The sum of these experimental results, which appear in the bias dependence of TMR and diff. TMR, should further stimulate spin-polarized transport theories at finite, large bias values beyond the first promising recent reports [18, 167, 169, 170] so as to address this difficult and complex theoretical problem.

A fundamental framework of Sp-SST requires an understanding of the role of the barrier band structure and electronic interaction with the FM electrodes, both in terms of induced magnetic moments on the barrier sites [81, 171], and on the dominant electronic character of the tunnelling current (see, e.g., the discussion on the Fe/MgO(001) system in section 1). These aspects in turn control the sign and amplitude of a given interface P in MTJs. The large P of LSMO interfaces in MTJs has been used as a spin analyser to determine the sign of P of the opposing MTJ interface. Groundbreaking work in 1999 on the interface between Co and Al_2O_3, $SrTiO_3$ and $Ce_{0.69}La_{0.31}O_{1.845}$ [172] initially revealed the intrinsic difference between tunnelling across a conventional oxide, and a transition metal (TM) oxide, barrier. In recent experiments, TiO_2 and $LaAlO_3$ TM oxide barriers also revealed a negative sign of P for Co [173, 174], in agreement with the spin polarization of its d band. This can reflect the incidence of efficient 'd-character' wavefunction coupling at the interface, as well as efficient electron tunnelling with respect to the conduction band of these transition metal oxides with 'd-character'. We note that a positive P was recently observed at the interface between Co and multiferroic $BiFeO_3$ [175]. A future review of transition metal oxides in magnetic tunnel junctions will further emphasize these fundamental and technological opportunities.

We note that all these experimental results are contingent upon the possible influence of a chemically uncontrolled barrier/Co interface due to the sample preparation procedure. For instance, oxidized Co at the STO/Co interface in LSMO/STO/Co junctions [172] was revealed through EELS experiments [176], with possible repercussions on spintronic transport (e.g. interface states, a quantum well, sign of P etc). In this vein, the LSMO/STO interface was used, using Sp-SST, to probe the spintronic properties of the $STO/Co_{1-x}Cr_x$ interface for $0.04 < x < 0.2$ [145]. Such MTJs were systematically found to be unstable electrically, and for large Cr concentrations, a spintronically dead MTJ could be crafted through large negative/positive applied bias values to yield a negative/positive sign of the effective $STO/Co_{1-x}Cr_x$ interfacial spin polarization [177]. Oxygen vacancies within the STO barrier, presumably created through the strong enthalpy of oxidation of adjacent Cr sites, were found to underscore this dramatic difference in device response between stable LSMO/STO/Co junctions and those with a CoCr counter-electrode. The ability to craft the resistive and magnetoresistive properties of a MTJ opens up vast possibilities, e.g. to electrochemically engineer an effective MTJ interface with interesting spintronic properties from the elemental constituents of the nominally grown interface. These results fall within a recent focus on the role of defects in the spintronics of semiconducting spacers (see, e.g., the citations of [178]). A future review of such bias-crafting effects within this research context will emphasize new opportunities for fundamental and applied spintronics research.

Finally, due to their chemical stability, manganites have been integrated into hybrid heterostructures that comprise organic semiconductor layers. For instance, a large magnetoresistance was obtained in the $LSMO/Alq_3/Co$ (Alq_3 = 8-hydroxy-quinoline aluminium) [15], thereby validating this organic semiconductor for spintronics, and this despite repeated cleaning of the LSMO surface with a solvent. Further results were obtained on this spacer [16] but also on carbon nanotubes [179]. This shows the potential for manganites to reveal novel spintronic effects across organic semiconductor and molecular spacers.

7. Conclusion and outlook

We have shown how the integration of half-metallic manganites into magnetic tunnel junctions could lead to active interfaces with the desired experimental half-metallic property for spintronics. We measure a tunnelling spin polarization at $T = 4$ K at $La_{2/3}Sr_{1/3}MnO_3/SrTiO_3$ (LSMO/STO) interfaces of type $MnO_2/La_{2/3}Sr_{1/3}O/TiO_2$ that can reach 95% through measurements at low bias, and up to 99% at larger bias. Our experiments peg the mobility

edge of the t_{2g} minority band at an energy of 340 ± 40 meV above the Fermi level. These conclusions apply to the interfacial LSMO band structure along the Γ–X direction as reflected by predominant tunnelling transmission through the STO barrier along Γ–M directions. Furthermore, our experiments ascribe exclusively the e_g electronic symmetry to any remaining minority states at the Fermi level, whether localized or not, at precisely the Γ point of interfacial LSMO where possible deviations from half-metallic behaviour for this manganite are predicted [113]. Given the spin-polarized solid-state tunnelling technique used here, these results reflect the probing of all states regardless of their mobility. The extent of our results is not affected by symmetry-filtering considerations. Our experimental results rule out localized states to describe the possible deviation from ideal half-metallicity, thereby helping to refine the present theoretical description of the electronic structure at such promising LSMO/STO interfaces [102]. They confirm the LSMO/STO candidate as a model system at the intersection between theory and experiment where it is possible to observe essentially half-metallic properties.

Our experimental results essentially validate the compact that studying the half-metallic class of materials would lead to large spintronic effects, and thus to an improved fundamental understanding of spintronics. However, successful applications of half-metals need to overcome the fact that manganites such as $La_{2/3}Sr_{1/3}MnO_3$ have at most a Curie temperature of only 360 K, which drops below room temperature at the interface [142]. Furthermore, as a crucial fact that has often been overlooked, double exchange half-metals do not effectively display half-metallic properties above $T \simeq T_C/3$ [94, 180]. This implies a renewed search for half-metals with $T_C \gg 300$ K, such as the encouraging candidate $LaSrTiO_3$:Co [181] with a Curie temperature $T_C = 450$ K. Exciting results have recently been obtained on the integration of the promising Co_2MnSi Heusler alloy with $T_C > 600$ K into Al_2O_3 junctions that yield 600% TMR [158]. These results fall into the current research trend of identifying interfaces between half-metallic systems and semiconductors that are most likely to retain the half-metallic property. The reader may find more information on this research direction in the contribution of Galanakis and Mavropoulos to this special edition on half-metals.

Beyond an enhanced fundamental comprehension of strongly correlated electron systems such as manganites, the allure of half-metals toward fundamental, let alone technological, spintronics is from here on directly challenged by the relentless progress of symmetry-filtered spintronics, with MgO(001)-based junctions now reaching 800% TMR [182], which corresponds to an effective $P = 89\%$. To address this challenge, it is important to utilize the symmetry polarization that generally underscores the spin polarization in half-metallic materials and perform groundbreaking studies of the symmetry-filtered spintronics effects themselves [7]. This predicted trend will likely go alongside a broad expansion of work on tunnelling from half-metals across transition metal oxides and molecular spacers [14] but also across multiferroic (or magnetoelectronic) [183] materials, as was reported recently [184], with an aim of electrically controling the magnetic properties of the half-metallic materials.

Acknowledgments

We are deeply indebted to all our colleagues at UMP CNRS/Thales at Orsay, the Laboratoire de Physique des Solides at Orsay, the Politecnico de Milano and FZ Jülich for stimulating discussions and research assistance, and in particular to Y Lemaître, F Ciccacci, L Duò and A Fert. M B thanks M Alouani, W Temmerman, P Dowben, M Coey, and Ph Mavropoulos for stimulating discussions. M B gratefully acknowledges the financing of his PhD, which led to many of the above results, through an Eiffel scholarship from the French ministry of Foreign Affairs. This work was partially supported by the AMORE European Contract

(G5RD-CT-2000-00138) and the 'Computational Magnetoelectronics' RTN. MB recognizes and appreciates the personal support of C Trippel and of Noah.

The reproduction/adaptation of several figures has been made with the permission of the publisher and at least one of the authors.

References

[1] Grünberg P, Schreiber R and Pang Y 1986 *Phys. Rev. Lett.* **57** 2442
[2] Baibich M N, Broto J M, Fert A, NguyenVanDau F, Petroff F, Etienne P, Creuzet G, Friedrich A and Chazelas J 1988 *Phys. Rev. Lett.* **61** 2472
[3] Wolf S A, Awschalom D D, Buhrman R A, Daughton J M, von Molnár S, Roukes M L, Chtchelkanova A Y and Treger D M 2001 *Science* **294** 1488
[4] Ortega J, Himpsel F, Mankey G and Willis R 1993 *Phys. Rev.* B **47** 1540
[5] Moodera J S, Kinder L R, Wong T M and Meservey R 1995 *Phys. Rev. Lett.* **74** 3273
[6] Yuasa S, Nagahama T and Suzuki Y 2002 *Science* **297** 234
[7] Bowen M, Barthélémy A, Bellini V, Bibes M, Jacquet E, Contour J and Dederichs P 2006 *Phys. Rev.* B **73** 140408(R)
[8] Faure-Vincent J, Tiusan C, Bellouard C, Popova E, Hehn M, Montaigne F and Schuhl A 2002 *Phys. Rev. Lett.* **89** 107206
[9] Katayama T, Yuasa S, Velev J, Zhuravlev M Y, Jaswal S and Tsymbal E 2006 *Appl. Phys. Lett.* **89** 112503
[10] Nader Y, Mény C, Bengone O and Panissod P 2006 *Phys. Rev. Lett.* **97** 257206
[11] Aviram A and Ratner M A 1974 *Chem. Phys. Lett.* **29** 277
[12] Liang W, Shores M, Bockrath M, Long J and Park H 2002 *Nature* **417** 725
[13] Champagne A, Pasupathy A and Ralph D 2005 *Nano Lett.* **5** 305
[14] Rocha A R, Garcia-Suarez V M, Bailey S, Lambert C, Ferrer J and Sanvito S 2005 *Nat. Mater.* **4** 335
[15] Xiong Z, Wu D, Vardeny Z and Shi J 2004 *Nature* **427** 821
[16] Wu D, Xiong Z H, Li X G, Vardeny Z V and Shi J 2005 *Phys. Rev. Lett.* **95** 016802
[17] Vázquez H, Oszwaldowski R, Pou P, Ortega J, Pérez R, Flores F and Kahn A 2004 *Europhys. Lett.* **65** 802
[18] Rocha A R, Garcia-Suarez V M, Bailey S, Lambert C, Ferrer J and Sanvito S 2006 *Phys. Rev.* B **73** 085414
[19] Moodera J S, Hao X, Gibson G A and Meservey R 1988 *Phys. Rev. Lett.* **61** 637
[20] LeClair P, Ha J K, Swagten H J M, Kohlhepp J T, van de Vin C H and de Jonge W J M 2002 *Appl. Phys. Lett.* **80** 625
[21] Gajek M, Bibes M, Barthélémy A, Bouzehouane K, Fusil S, Varela M, Fontcuberta J and Fert A 2005 *Phys. Rev.* B **72** 020406(R)
[22] Gajek M, Bibes M, Varela M, Fontcuberta J, Herranz G, Fusil S, Bouzehouane K, Barthélémy A and Fert A 2006 *J. Appl. Phys.* **99** 08E504
[23] Gajek M, Bibes M, Fusil S, Bouzehouane K, Fontcuberta J, Barthélémy A and Fert A 2006 *Preprint* cond-mat/0606444
[24] Chapline M G and Wang S X 2006 *Phys. Rev.* B **74** 014418
[25] Lüders U, Bibes M, Bouzehouane K, Jacquet E, Contour J-P, Fusil S, Bobo J-F, Fontcuberta J, Barthélémy A and Fert A 2006 *Appl. Phys. Lett.* **88** 082505
[26] Lüders U, Barthélémy A, Bibes M, Bouzehouane K, Fusil S, Jacquet E, Contour J-P, Bobo J-F, Fontcuberta J and Fert A 2006 *Adv. Mater.* **18** 1733
[27] Bowen M *et al* 2001 *Appl. Phys. Lett.* **79** 1655
[28] Faure-Vincent J, Tiusan C, Jouguelet E, Canet F, Sajieddine M, Bellouard C, Popova E, Hehn M, Montaigne F and Schuhl A 2003 *Appl. Phys. Lett.* **82** 4507
[29] Yuasa S, Nagahama T, Fukushima A, Suzuki Y and Ando K 2004 *Nat. Mater.* **3** 868
[30] Parkin S, Kaiser C, Panchila A, Rice P M, Hughes B, Samant M and Yang S 2004 *Nat. Mater.* **3** 862
[31] Yuasa S, Fukushima A, Kubota H, Suzuki Y and Ando K 2006 *Appl. Phys. Lett.* **89** 042505
[32] Butler W H, Zhang X G, Schulthess T C and MacLaren J M 2001 *Phys. Rev.* B **63** 054416
[33] Mathon J and Umerski A 2001 *Phys. Rev.* B **63** 220403(R)
[34] Jullière M 1975 *Phys. Lett.* A **54** 225
[35] de Groot R A, Mueller F M, van Engen P G and Buschow K H J 1983 *Phys. Rev. Lett.* **50** 2024
[36] Coey M, Viret M and von Molnár S 1999 *Adv. Phys.* **48** 167
[37] Zener C 1951 *Phys. Rev.* **82** 403
[38] Goodenough J 1955 *Phys. Rev.* **100** 564
[39] Goodenough J, Wold A, Arnott R and Menyuk N 1961 *Phys. Rev.* **124** 373
[40] Goodenough J 1976 *Magnetism and the Chemical Bond* (Huntington: Krieger)

[41] Anderson P and Hasegawa H 1955 *Phys. Rev.* **100** 675
[42] Kubo K and Ohata N 1972 *J. Phys. Soc. Japan* **33** 21
[43] Millis A, Littlewood P and Shraiman B 1995 *Phys. Rev. Lett.* **74** 5144
[44] Zhao G, Conder K, Keller H and Muller K 1996 *Nature* **381** 676
[45] Jahn A and Teller E 1937 *Proc. R. Soc.* A **161** 220
[46] Millis A 1998 *Nature* **392** 147
[47] Bibes M, Balcells L, Valencia S, Fontcuberta J, Wojcik M, Jedryka E and Nadolski S 2001 *Phys. Rev. Lett.* **87** 067210
[48] Dagotto E, Hotta T and Moreo A 2001 *Phys. Rep.* **344** 1
[49] Dörr K 2006 *J. Phys. D: Appl. Phys.* **39** R125
[50] von Helmolt R, Wecker J, Holzapfel B, Schultz L and Samwer K 1993 *Phys. Rev. Lett.* **71** 2331
[51] Martin M C, Shirane G, Endoh Y, Hirota K, Moritomo Y and Tokura Y 1996 *Phys. Rev.* B **53** 14285
[52] Hartinger C, Mayr F, Loidl A and Kopp T 2004 *Phys. Rev.* B **70** 134415
[53] Ogale S B, Talyansky V, Chen C H, Ramesh R, Greene R L and Venkatesan T 1996 *Phys. Rev. Lett.* **77** 1159
[54] Pallecchi I, Pellegrino L, Bellingeri E, Siri A S and Marre D 2005 *Phys. Rev.* B **71** 014406
[55] Thiele C, Dörr K, Fähler S, Schultz L, Meyer D, Levin A and Paufler P 2005 *Appl. Phys. Lett.* **87** 262502
[56] Wu T, Ogale S B, Garrison J E, Nagaraj B, Biswas A, Chen Z, Greene R L, Ramesh R, Venkatesan T and Millis A J 2001 *Phys. Rev. Lett.* **86** 5998
[57] Hong X, Posadas A, Lin A and Ahn C H 2003 *Phys. Rev.* B **68** 134415
[58] Inoue I 2005 *Semicond. Sci. Technol.* **20** S1121
[59] Mitra C, Raychaudhuri P, Köbernik G, Dörr K, Müller K-H, Schultz L and Pinto R 2001 *Appl. Phys. Lett.* **79** 2408
[60] Mitra C, Raychaudhuri P, Dorr K, Muller K-H, Schultz L, Oppeneer P M and Wirth S 2003 *Phys. Rev. Lett.* **90** 017202
[61] Sheng Z, Song W, Suna Y, Sun J and Shen B 2005 *Appl. Phys. Lett.* **87** 032501
[62] Ruzmetov D, Seo Y, Belenky L J, Kim D-M, Ke X, Sun H, Chandrasekhar V, Eom C-B, Rzchowski M S and Pan X 2005 *Adv. Mater.* **17** 2869
[63] Takamura Y, Chopdekar R, Scholl A, Doran A, Liddle J, Harteneck B and Suzuki Y 2006 *Nano Lett.* **6** 1287
[64] Nikolaev K, Dobin A, Krivorotov I, Cooley W, Bhattacharya A, Kobrinskii A L, Glazman L, Wentzovitch R, Dahlberg E D and Goldman A M 2000 *Phys. Rev. Lett.* **85** 3728
[65] Krivorotov I, Nikolaev K, Dobin A, Goldman A and Dahlberg E 2001 *Phys. Rev. Lett.* **86** 5779
[66] Ohsawa T, Kubota S, Itoh H and Inoue J 2005 *Phys. Rev.* B **71** 212407
[67] Izumi M, Ogimoto Y, Okimoto Y, Manako T, Ahmet P, Nakajima K, Chikyow T, Kawasaki M and Tokura Y 2001 *Phys. Rev.* B **64** 064429
[68] Sahana M, Dörr K, Walter T, Nenkov K, Eckert D and Müller K 2002 *IEEE Trans. Magn.* **38** 2904
[69] Katine J A, Albert F J, Buhrman R A, Myers E B and Ralph D C 2000 *Phys. Rev. Lett.* **84** 3149
[70] Sun J, Abraham D, Rao R and Eom C 1999 *Appl. Phys. Lett.* **74** 3017
[71] Pellecchi I, Pellegrino L, Caviglia A, Bellingeri E, Canu G, Gazzadi G C, Siri A S and Marré D 2006 *Phys. Rev.* B **74** 014434
[72] Pallecchi I, Pellegrino L, Caviglia A, Bellingeri E, Canu G, Gazzadi G C, Siri A S and Marre D 2006 *Phys. Rev.* B **74** 014434
[73] Céspedes O, Watts S, Coey J M D, Dörr K and Ziese M 2005 *Appl. Phys. Lett.* **87** 083102
[74] Talbayev D, Zhao H, Lupke G, Venimadhav A and Li Q 2006 *Phys. Rev.* B **73** 014417
[75] Sun J, Gallagher W, Ducombe P, Krusin-Elbaum L, Altman R, Gupta A, Lu Y, Gong G and Xiao G 1996 *Appl. Phys. Lett.* **69** 3266
[76] Sun J, Krusin-Elbaum L, Duncombe P, Gupta A and Laibowitz R 1997 *Appl. Phys. Lett.* **70** 1769
[77] Viret M, Drouet M, Nassar J, Contour J, Fermon C and Fert A 1997 *Europhys. Lett.* **39** 545
[78] Jo M-H, Mathur N, Evetts J and Blamire M 2000 *Appl. Phys. Lett.* **77** 3803
[79] Jo M-H, Mathur N and Blamire M 2002 *Appl. Phys. Lett.* **80** 2722
[80] Barthelemy A *et al* 2002 *J. Magn. Magn. Mater.* **242** 68
[81] Tsymbal E, Mryasov O and LeClair P 2003 *Phys. Lett.* **15** R109
[82] Haghiri-Gosnet A, Arnal T, Soulimane R, Koubaa M and Renard J 2004 *Phys. Status Solidi* a **201** 1392
[83] Bobo J, Gabillet L and Bibes M 2004 *J. Phys.: Condens. Matter* **16** S471
[84] Zutíc I, Fabian J and Sarma S D 2004 *Rev. Mod. Phys.* **76** 323
[85] Schuhl A and Lacour D 2005 *C. R. Physique* **6** 945
[86] Imada M, Fujimori A and Tokura Y 1998 *Rev. Mod. Phys.* **70** 1039
[87] Tokura Y and Tomioka Y 1999 *J. Magn. Magn. Mater.* **200** 1
[88] Ziese M 2002 *Rep. Prog. Phys.* **65** 143

[89] Haghiri-Gosnet A-M and Renard J-P 2003 *J. Phys. D: Appl. Phys.* **36** R127
[90] Nadgorny B, Mazin I I, Osofsky M, Soulen J R J, Broussard P, Stroud R M, Singh D J, Harris V G, Arsenov A and Mukovskii Y 2001 *Phys. Rev.* B **63** 184433
[91] Calderón M, Brey L and Guinea F 1999 *Phys. Rev.* B **60** 6698
[92] Skomski R and Dowben P A 2002 *Europhys. Lett.* **58** 544
[93] Sasioglu E, Sandratskii L M, Bruno P and Galanakis I 2005 *Phys. Rev.* B **72** 184415
[94] Lezaic M, Mavropoulos P, Enkovaara J, Bihlmayer G and Blugel S 2006 *Phys. Rev. Lett.* **97** 026404
[95] Mavropoulos P, Sato K, Zeller R, Dederichs P H, Popescu V and Ebert H 2004 *Phys. Rev.* B **69** 054424
[96] Edwards D and Hertz J 1973 *J. Phys. F: Met. Phys.* **3** 2191
[97] Irkhin V Y and Katsnel'son M I 1983 *Sov. Phys.—Solid State* **25** 1947
[98] Chioncel L, Katsnelson M I, de Groot R A and Lichtenstein A I 2003 *Phys. Rev.* B **68** 144425
[99] de Wijs G A and de Groot R A 2001 *Phys. Rev.* B **64** 020402
[100] Nagao K, Miura Y and Shirai M 2006 *Phys. Rev.* B **73** 104447
[101] Mavropoulos P, Lezaic M and Blugel S 2005 *Phys. Rev.* B **72** 174428
[102] Zenia H, Gehring G and Temmerman W 2007 *New J. Phys.* **9** 105 (*Preprint* cond-mat/0604343)
[103] Galanakis I, Lezaic M, Bihlmayer G and Blugel S 2005 *Phys. Rev.* B **71** 214431
[104] Yamada H, Ogawa Y, Ishii Y, Sato H, Kawasaki M, Akoh H and Tokura Y 2004 *Science* **305** 646
[105] Kumigashira H *et al* 2006 *Appl. Phys. Lett.* **88** 192504
[106] Maurice J-L, Imhoff D, Contour J-P and Colliex C 2006 *Phil. Mag.* **86** 2127
[107] Ishii Y, Yamada H, Sato H, Akoh H, Ogawa Y, Kawasaki M and Tokura Y 2006 *Appl. Phys. Lett.* **89** 042509
[108] Banach G and Temmerman W M 2004 *Phys. Rev.* B **69** 054427
[109] Zenia H, Gehring G A, Banach G and Temmerman W M 2005 *Phys. Rev.* B **71** 024416
[110] Kavich J, Warusawithana M, Freeland J, Ryan P, Zhai X, Kodama R and Eckstein J 2006 *Preprint* cond-mat/0512158
[111] Kotliar G, Savrasov S Y, Haule K, Oudovenko V S, Parcollet O and Marianetti C A 2006 *Rev. Mod. Phys.* **78** 865
[112] Pickett W and Singh D 1997 *Phys. Rev.* B **55** R8642
[113] Livesay E, West R, Dugdale S, Santi G and Jarlborg T 1999 *J. Phys.: Condens. Matter* **11** L279
[114] Bak T, Nowotny J, Rekas M and Sorrell C 2001 *J. Phys. Chem. Solids* **62** 737
[115] Park J-H, Vescovo E, Kim H-J, Kwon C, Ramesh R and Venkatesan T 1998 *Phys. Rev. Lett.* **81** 1953
[116] Park J-H, Vescovo E, Kim H-J, Kwon C, Ramesh R and Venkatesan T 1998 *Nature* **392** 794
[117] Lyonnet R 2000 *PhD Thesis* Université de Paris XI Orsay, France
[118] Maurice J-L, Lyonnet R and Contour J-P 2000 *J. Magn. Magn. Mater.* **211** 91
[119] Lyonnet R, Maurice J-L, Hytch M, Michel D and Contour J-P 2000 *Appl. Surf. Sci.* **162/163** 245
[120] Pailloux F, Lyonnet R, Maurice J-L and Contour J-P 2001 *Appl. Surf. Sci.* **177** 263
[121] Maurice J, Pailloux F, Barthélémy A, Rocher A, Durand O, Lyonnet R and Contour J 2002 *Appl. Surf. Sci.* **188** 176
[122] Samet L, Imhoff D, Maurice J-L, Contour J-P, Gloter A, Manoubi T, Fert A and Colliex C 2003 *Euro. Phys. J.* B **34** 179
[123] Maurice J-L, Pailloux F, Barthélémy A, Durand O, Imhoff D, Lyonnet R, Rocher A and Contour J-P 2003 *Phil. Mag.* **83** 3201
[124] Bertacco R, Contour J and Barthélémy A 2002 *Surf. Sci.* **511** 366
[125] Rijnders G, Blank D, Choi J and Eom C-B 2004 *Appl. Phys. Lett.* **84** 505
[126] Bellini V 2000 *PhD Thesis* Rheinisch-Westfälischen Technischen Hochschule Aachen, p 121
[127] Bowen M, Barthélémy A, Bibes M, Jacquet E, Contour J-P, Fert A, Ciccacci F, Duò L and Bertacco R 2005 *Phys. Rev. Lett.* **95** 137203
[128] Higuchi T, Tsukamoto T, Sata N, Ishigame M, Tezuka Y and Shin S 1998 *Phys. Rev.* B **57** 6978
[129] Higuchi T, Nozawa S, Tsukamoto T, Ishii H, Eguchi R, Tezuka Y, Yamaguchi S, Kanai K and Shin S 2002 *Phys. Rev.* B **66** 153105
[130] Zhuang M, Zhang W and Ming N 1997 *Phys. Rev.* B **56** 14547
[131] Mazin I 1999 *Phys. Rev. Lett.* **83** 1427
[132] Wortmann D, Ishida H and Blugel S 2005 *Phys. Rev.* B **72** 235113
[133] Mavropoulos P, Papanikolaou N and Dederichs P H 2000 *Phys. Rev. Lett.* **85** 1088
[134] Aiura Y, Hase I, Bando H, Yasue T, Saitoh T and Dessau D S 2002 *Surf. Sci.* **515** 61
[135] Tersoff J 1984 *Phys. Rev. Lett.* **52** 465
[136] Velev J P, Belashchenko K D, Stewart D A, van Schilfgaarde M, Jaswal S S and Tsymbal E Y 2005 *Phys. Rev. Lett.* **95** 216601
[137] Montaigne F, Nassar J, Vaurès A, Dau F N V, Petroff F, Schuhl A and Fert A 1998 *Appl. Phys. Lett.* **73** 2829

[138] Dörr K, de Teresa J, Müller K, Eckert D, Walter T, Vlakho E, Nenkov K and Schultz L 2000 *J. Phys.: Condens. Matter* **12** 7099
[139] Bowen M, Bibes M, Barthélémy A, Contour J-P, Anane A, Lemaître Y and Fert A 2003 *Appl. Phys. Lett.* **82** 233
[140] van de Veerdonk R, Nowak J, Meservey R, Moodera J and de Jonge W 1997 *Appl. Phys. Lett.* **71** 2839
[141] Ishii Y, Yamada H, Sato H, Akoh H, Kawasaki M and Tokura Y 2005 *Appl. Phys. Lett.* **87** 022509
[142] Garcia V, Bibes M, Barthélémy A, Bowen M, Jacquet E, Contour J-P and Fert A 2004 *Phys. Rev.* B **69** 052403
[143] Bardeen J 1961 *Phys. Rev. Lett.* **6** 57
[144] Zhang S, Levy P M, Marley A C and Parkin S S P 1997 *Phys. Rev. Lett.* **79** 3744
[145] Bowen M 2003 *PhD Thesis* Université de Paris-XI Orsay, France http://tel.ccsd.cnrs.fr/perl/searchfr?&authors=Bowen,Martin&L%ANG=fr
[146] Moodera J, Nowak J and van de Veerdonk R J 1998 *Phys. Rev. Lett.* **80** 2941
[147] Nagahama T, Yuasa S, Suzuki Y and Tamura E 2001 *Appl. Phys. Lett.* **79** 4381
[148] Antonov V N, Harmon B N, Yaresko A N, Bekenov L V and Shpak A P 2006 *Phys. Rev.* B **73** 094445
[149] Gebauer R and Car R 2004 *Phys. Rev. Lett.* **93** 160404
[150] Kurth S, Stefanucci G, Almbladh C-O, Rubio A and Gross E K U 2005 *Phys. Rev.* B **72** 035308
[151] Maciejko J, Wang J and Guo H 2006 *Phys. Rev.* B **74** 085324
[152] Calderón M J and Brey L 2001 *Phys. Rev.* B **64** 140403
[153] Akimoto T, Moritomo Y, Nakamura A and Furukawa N 2000 *Phys. Rev. Lett.* **85** 3914
[154] Bowen M, Barthélémy A, Bibes M, Jacquet E, Contour J-P, Fert A, Wortmann D and Blügel S 2005 *J. Phys.: Condens. Matter* **17** L407
[155] Pickett W and Singh D 1998 *Phys. Rev.* B **57** 88
[156] Bratkovsky A 1997 *Phys. Rev.* B **56** 2344
[157] Bertacco R, Portalupi M, Marcon M, Duò L, Ciccacci F, Bowen M, Contour J and Barthélémy A 2002 *J. Magn. Magn. Mater.* **242–245** 710
[158] Sakuraba Y, Hattori M, Oogane M, Ando Y, Kato H, Sakuma A, Miyazaki T and Kubota H 2006 *Appl. Phys. Lett.* **88** 192508
[159] Sakuraba Y, Miyakoshi T, Oogane M, Ando Y, Sakuma A, Miyazaki T and Kubota H 2006 *Appl. Phys. Lett.* **89** 052508
[160] Fowler R and Nordheim L 1928 *Proc. R. Soc.* **119** 173
[161] Gundlach K-H 1973 *J. Appl. Phys.* **44** 5006
[162] Ohtomo A, Müller D, Grazul J and Hwang H 2002 *Nature* **419** 378
[163] Nagahama T, Yuasa S, Tamura E and Suzuki Y 2005 *Phys. Rev. Lett.* **95** 086602
[164] D H *et al* 2007 submitted
[165] Montaigne F 1999 *PhD Thesis* Université de Paris XI-Orsay, France
[166] Qiu Z and Smith N 2002 *J. Phys.: Condens. Matter* **14** R169
[167] Levy P M and Fert A 2006 *Phys. Rev. Lett.* **97** 097205
[168] Fuchs G D, Katine J A, Kiselev S I, Mauri D, Wooley K S, Ralph D C and Buhrman R A 2006 *Phys. Rev. Lett.* **96** 186603
[169] Zhang C, Zhang X-G, Krstić P S, Cheng H P, Butler W H and MacLaren J M 2004 *Phys. Rev.* B **69** 134406
[170] Theodonis I, Kioussis N, Kalitsov A, Chshiev M and Butler W 2006 *Phys. Rev. Lett.* **97** 237205
[171] Bowen M, Cros V, Jaffres H, Bencok P, Petroff F and Brookes N B 2006 *Phys. Rev.* B **73** 012405
[172] Teresa J D, Barthélémy A, Fert A, Contour J, Montaigne F and Seneor P 1999 *Science* **286** 507
[173] Bibes M, Bowen M, Barthélémy A, Anane A, Bouzehouane K, Carretero C, Jacquet E, Contour J-P and Durand O 2003 *Appl. Phys. Lett.* **82** 3269
[174] Garcia V, Bibes M, Maurice J-L, Jacquet E, Bouzehouane K, Contour J-P and Barthélémy A 2005 *Appl. Phys. Lett.* **87** 212501
[175] Béa H *et al* 2006 *Preprint* cond-mat/0607563
[176] Maurice J-L, Pailloux F, Imhoff D, Contour J-P, Barthélémy A, Bowen M, Colliex C and Fert A 2003 *MRS Proc.* **746** 145
[177] Bowen M, Maurice J-L, Barthélémy A, Prodhomme P, Jacquet E, Contour J-P, Imhoff D and Colliex C 2006 *Appl. Phys. Lett.* **89** 103517
[178] Tsymbal E, Sokolov A, Sabirianov I F and Doudin B 2003 *Phys. Rev. Lett.* **90** 186602
[179] Hueso L E *et al* 2006 *Appl. Phys. Lett.* **88** 083120
[180] Itoh H, Oshawa T and Inoue J 2000 *Phys. Rev. Lett.* **84** 2501
[181] Herranz G *et al* 2006 *Phys. Rev. Lett.* **96** 027207
[182] Hayakawa J, Ikeda S, Lee Y, Matsukura F and Ohno H 2006 *Appl. Phys. Lett.* **89** 232510
[183] Wang J *et al* 2003 *Science* **299** 1719
[184] Bea H *et al* 2006 *Appl. Phys. Lett.* **89** 242114